PNAS
www.pnas.org

Supplementary Information for

Comparative transcriptomics of 3 high-altitude passerine birds and their low-altitude relatives

Yan Hao[a,b], Ying Xiong[a,b], Yalin Cheng[a,b], Gang Song[a], Chenxi Jia[a], Yanhua Qu[a,1], and Fumin Lei[a,b,c,1]

[a]Key Laboratory of Zoological Systematics and Evolution, Institute of Zoology, Chinese Academy of Sciences, Beijing 100101, China; [b]College of Life Science, University of Chinese Academy of Sciences, Beijing 100049, China; and [c]Center for Excellence in Animal Evolution and Genetics, Chinese Academy of Sciences, Kunming 650223, China

[1]To whom correspondence may be addressed. Email: quyh@ioz.ac.cn or leifm@ioz.ac.cn.

This PDF file includes:

Supplementary text
Figs. S1 to S14
Tables S1 to S12
Caption for database S1
References for SI reference citations

Other supplementary materials for this manuscript include the following:

Dataset S1

www.pnas.org/cgi/doi/10.1073/pnas.1819657116

Supplementary Information Text

Materials and Methods

Ethics Statement. All samples were collected and all experiments were conducted in accordance with the regulations of the ethics committee of the Institute of Zoology, Chinese Academy of Sciences, Beijing, China, with authorization from the local forestry authorities, and in compliance with the National Wildlife Conservation Law of China. Voucher specimens were cataloged in the ornithological collection of the National Zoological Museum, Institute of Zoology, Chinese Academy of Sciences, Beijing, China.

Specimen Collection, RNA Extraction, and Transcriptome Sequencing. All 6 species used in this study are resident passerines in 2 families within the order Passeriformes: the gray-crested tit (*Lophophanes dichrous*), the rufous-vented tit (*Periparus rubidiventris*), the marsh tit (*Poecile palustris*), and the yellow-bellied tit (*Pardaliparus venustulus*) in the family Paridae; and the rufous-fronted tit (*Aegithalos iouschistos*) and the black-throated tit (*A. concinnus*) in the family Aegithalidae (1–3). The high-altitude species, all native to the Qinghai-Tibet Plateau (QTP), were *L. dichrous* (2,300–4,600 m above sea level), *Pe. rubidiventris* (2,400–4,300 m), and *A. iouschistos* (2,700–4,300 m) (1–3). The closely related species, generally distributed in low altitudes in East Asia, were *Po. palustris* (0–2,100 m), *Pa. venustulus* (0–2,000 m), and *A. concinnus* (0–2,500 m) (1–3). High-altitude species were collected on the QTP, and low-altitude species were collected in eastern China (Fig. 1*A*; Table S1). We collected 4 to 5 adults of each of the 6 tit species using mist nets on autumn 2015 and autumn 2016 (Table S1). Birds were killed by thoracic compression and we collected 5 tissues (cardiac muscle, flight muscle, liver, lung, and kidney) known to be associated with metabolic performance and oxygen utilization (4, 5). These tissues were immediately placed in the RNA preservative RNAhold (TransGen, Beijing, China), and stored at −80°C. Total RNA was extracted using the EASYspin Fibrous Tissue RNA Mini Kit (Aidlab Biotech, Beijing, China), following the manufacturer's instructions. The quality of

each RNA sample was examined with an Agilent 2100 Bioanalyzer (Agilent Technologies, Palo Alto, CA, USA). mRNA was isolated using Oligo (dT) magnetic beads, and fragmented for cDNA synthesis. After purification and end repair, nucleotide A (adenine) was added, the mRNA fragments were connected using adapters, and amplified with PCR. All sample libraries were quantified and qualified using an Agilent 2100 Bioanalyzer (Agilent Technologies, Palo Alto, CA, USA) and an ABI StepOnePlus Real-Time PCR System (Applied Biosystems, Foster City, CA, USA) by the Beijing Genomics Institute (Shenzhen, China). Paired-end 150 bp libraries were sequenced with the Illumina HiSeq 4000 and Illumina HiSeq X Ten sequencing platforms (Table S1). Raw data were cleaned by removing reads with >10 bases aligned to the adapter sequences (allowing ≥10% mismatches), reads with ≥10% ambiguous bases ("N") and reads with >40% bases having a quality score <20, using SOAPnuke (version 1.5.3) (6).

De Novo Assembly, Mapping, and Quantification. Cleaned reads were combined into tissue groups for individual species, and assembled into transcriptomes de novo with Trinity (version 2.4.0) (7). All Trinity options were set to default except the minimum kmer coverage, which was set to 2 instead of 1; a minimum kmer coverage of 2 has been shown to increase application speed, reduce memory usage, and improve assembly accuracy (7). All transcripts were then filtered to reduce the impact of redundant, erroneous, nonexpressed, and poorly expressed transcripts. First, we clustered the transcript sequences and removed redundant transcripts using CD-HIT (version 4.6.8), setting word length to 10 and the sequence identity threshold to 0.95 (8). We then computed ExN50 statistic, a statistic measuring assembly quality, following the Trinity manual (http://trinityrnaseq.github.io) (7). The ExN50 is defined as the minimum contig length required to cover 50% of the transcriptome, based only on the most highly expressed transcripts (7). We also used Bowtie2 (version 2.3.2) to assess transcript quality, by mapping reads back to their respective transcriptomes (9). We used BUSCO (version 3.0.2) to determine transcriptome assembly completeness based on conserved avian orthologs (downloaded from

https://busco.ezlab.org/datasets/aves_odb9.tar.gz) (10). Second, we mapped all of the paired-end reads from each sample back to its own de novo transcriptome using RSEM (version 1.3.0) (11). We obtained the resulting fragments per kilobase of exon per million fragments mapped (FPKM). For each species, we retained only transcripts where FPKM was >1 in at least half of all samples from any one tissue.

Ortholog Identification and Functional Annotation. We selected the zebra finch (*Taeniopygia guttata*) as an outgroup (12). This species belongs to the Estrildidae, a family more primitive than the Paridae and the Aegithalidae in avian phylogenetic tree (13). The coding sequences (CDSs) and protein sequences of the zebra finch were downloaded from Ensembl (http://ftp.ensembl.org/pub/release-91/fasta/taeniopygia_guttata/) (14). For each unique gene, only the longest transcript and protein sequence were retained. One-to-one orthologs among all 6 tit species and the zebra finch were identified using the reciprocal best-hit method in BLASTn (version 2.6.0+), with an E value cutoff of 1e-10 and a minimum percentage identity of 30%. When best-hit values were equivalent for more than one result, we chose the longest transcript. Orthologous protein sequences of the zebra finch were used as proxies for searches against protein databases [NCBI nonredundant (NR) and Swiss-Prot] with BLASTp (version 2.6.0+; setting the E value cutoff to 1e-5 and the maximum number of blast hits to 20). The best hit was considered the final annotation. The NR results were used as input for Blast2GO PRO (version 4.1.9) (15) to determine Gene Ontology (GO) terms and InterPro IDs. The Kyoto Encyclopedia of Genes and Genomes (KEGG) orthology of each protein was determined with the KAAS-KEGG Automatic Annotation Server (http://www.genome.jp/tools/kaas/), using the Bi-directional Best Hit (BBH) method (16).

Sequence Alignment. We identified the CDSs in each of the 6 tits by aligning the orthologous protein sequences of the zebra finch to the orthologous gene sequences of each tit, using

Exonerate (version 2.2.0) with the model protein2genome (17). All orthologous CDSs were aligned by codon using Prank (version 170427) (18); branch-site likelihood ratio tests for positive selection in Prank have been shown to be more accurate than those of ClustalW, MAFFT, and Muscle (18, 19). We used Gblocks (version 0.91b) (20) in codon mode to eliminate poorly aligned codons, gaps, ambiguous bases ("N"), and sequences <75 bp long, so as to avoid overestimating the rate of nonsynonymous substitutions. The remaining high-confidence alignments were used for all downstream analyses: the phylogenetic analysis was based on both mitochondrial and nuclear genes, whereas tests of positive selection, genomic convergence were only based on nuclear genes.

Phylogenetic Analysis. The nucleotide sequence alignments of all orthologous genes were concatenated to form a super-alignment. Because 4-fold-degenerate (4D) sites are regarded as neutral and free from selective constraints (21, 22), we extracted the 4D sites from the super-alignment using a custom script. We used jModeltest (version 2.1.10) (23) to determine the best-fit model of the nucleotide substitution for the concatenated 4D sites, based on the Akaike information criterion (AIC). RAxML (version 8.2.10) (24) was used to reconstruct a maximum likelihood (ML) phylogeny with 1,000 bootstrap replicates, and FigTree (version 1.4.2) (http://tree.bio.ed.ac.uk/software/figtree/) was used to visualize the topology.

Identification of Positive Selection. Using our ML topology as a guide, we ran 7 different branch-site likelihood ratio tests (LRTs) to identify positively selected genes, setting 1 to 3 high-altitude lineages as the foreground branches (the branches of interest were specified a priori) (Table S5). The branch-site model (null model: model = 2, NSsites = 2, $\omega = 1$; alternative model: model = 2, NSsites = 2, $\omega = 1.4$) was implemented in the CODEML module of the PAML package (version 4.9) (25). We used Chi-square tests with 1 degree of freedom to evaluate differences in LRT results; $P < 0.05$ was considered significant. Genes shown to be under

positive selection were combined and considered candidates. The ratio of nonsynonymous substitutions per nonsynonymous site to synonymous substitutions per synonymous site (dN/dS) represents the rate at which a particular protein-coding sequence has evolved, indicating selective force of the gene (26). We used a one-ratio model (model = 0, NSsites = 0, $\omega = 1.4$) to estimate the overall dN/dS ratio for each ortholog to determine whether specific gene sets exhibited significant shifts in evolutionary rates, and whether altitude, ortholog expression, or connectivity (i.e., number of direct connections from one gene to other genes) correlated with evolutionary rate.

Detection of Genomic Convergence. Based on the amino acid sequences translated from all orthologous alignments and the ML tree topology, we reconstructed ancestral character states with CODEML (25), using the Empirical + F model, the Jones, Taylor, and Thorton (JTT) matrix, and a discrete gamma model for forty rate categories. We identified genes under convergence as those meeting 2 criteria: (*i*) identical amino acid residues in any 2 of the 3 high-altitude lineages, and (*ii*) for each of those 2 lineages, the identical amino acid residues differed from the homologous positions in the most recent common ancestor of each high- and low-altitude species pair. If the amino acid residues of the 2 most recent common ancestors of the high-altitude species were identical, they were considered "parallel" and if they were different, they were considered "converged". Both cases were considered to represent convergent evolution (27). The positions of convergent nonsynonymous amino acid substitutions were determined by comparison with the orthologous sequences of the zebra finch. To minimize the impact of random convergence, we used JTT-f_{gene} amino acid substitution models. First, the node sequences, branch lengths, relative evolutionary rates, and average amino acid frequencies across all sites were used to estimate the expected number of convergent sites in each ortholog, following Zou and Zhang (28). Second, a Poisson test was used to detect differences between the observed and expected number of convergent sites in each ortholog (where $P < 0.05$ was considered significant). Genes

were considered adaptively convergent genes if they not only had a nonrandom convergent change, but also if they had been subject to positive selection.

Normalization of Transcriptomic Data. To minimize the impact that gene expression differences were falsely detected due to artifacts, such as different number of transcripts and transcript lengths in 6 de novo transcriptome assemblies, we focused gene expression analyses on the one-to-one orthologs which had high-confidence alignments across the 6 species. We first trimmed these orthologs to the same lengths and calculated gene expression values by mapping all of the paired-end reads from each sample back to the trimmed orthologs of each species using RSEM (version 1.3.0) (3). We normalized gene expression data to allow the comparison of these data among biological replicates, tissues, and species. To compare gene expression values among replicates from the same tissue in the same species, we used the trimmed mean of M-value normalization (TMM), as implemented in the R package edgeR (version 3.16.5) (29). For comparisons among species and among tissues, we used scaling factors to normalize the expression levels of all orthologs across all samples (30, 31). That is, we first determined the median expression levels of the top 1,000 most conserved genes (i.e., lower coefficient of variance) in the interquartile range for each sample. Second, we identified the scaling factors that adjusted the median expression values to a common value. Third, we used these scaling factors to scale the gene expression levels of all sample. Our gene expression analyses were based on normalized expression data for the trimmed orthologs.

Expression Profile Analysis. We constructed a gene expression matrix with 128 columns, each representing a sample, and 7,048 lines, each corresponding to the expression of an ortholog. We used this matrix to calculate the Spearman's correlation coefficients between all pairs of samples. We used a nonparametric correlation because this method is less sensitive to outliers and inaccuracies caused in expression normalization. Hierarchical clustering of Spearman's

correlation coefficients between all pairs of samples across all genes was performed using the complete-linkage agglomerative method and the correlation distance metric. The symmetrical heat map of all samples was generated using the R package pheatmap (version 1.0.10).

Principal Component Analysis (PCA). Normalized gene expression data were log transformed. We performed a PCA on these transformed data using the R package gmodels (version 2.18.1). We performed 2 sets of PCAs: one PCA of the overall dataset, including samples from all 5 tissues across all 6 species and 5 separate PCAs on each of 5 tissues. For the first PCA, a one-way analysis of variance (ANOVA) was applied to each PC axis to detect the effects of tissue and species on the samples, using the R package stats (version 3.5.1). All *P* values were corrected for the effects of multiple tests using FDR (FDR < 0.05 was considered statistically significant) (32, 33).

Gene Expression Phylogeny Analysis. Pairwise distance between samples was calculated by 1 − Spearman's correlation coefficient. Gene expression tree for each tissue was reconstructed using neighbor joining approach in R package ape (version 5.1) according to the pairwise distance matrix (34). These neighbor-joining expression-based trees were visualized using FigTree (version 1.4.2).

Differentially Expressed Genes. We obtained differentially expressed genes using 4 methods to compare gene expression values between each of the 3 high- and low-altitude species pairs: R packages DESeq2 (version 1.14.1) (35), edgeR (version 3.16.5) (29), reproducibility-optimized test statistic (ROTS, version 1.2.0) (36), and limma (version 3.30.13) (37). For DESeq2 (35), we used DESeqDataSetFromMatrix to construct an object and DESeq to conduct differential expression analysis based on the negative binominal distribution. For edgeR (29), we used calcNormFactors to calculate normalization factors, estimateDisp to estimate common dispersion

and tagwise dispersion, and exactTest to determine expression differentiation. For ROTS (36), we used calcNormFactors in edgeR (29) to calculate normalization factors, voom in limma (37) to transform data, and ROTS to perform differential expression analysis (500 bootstrap permutations). For limma (37), we used calcNormFactors in edgeR (29) to calculate normalization factors, voom to transform data, lmFit to fit a linear model, and eBayes to compute moderated t-statistics for differential expression. Genes with a count-per-million >1, a 2-fold (or greater) change in relative expression between the high- and low-altitude species, and an FDR-adjusted $P < 0.05$ were deemed differentially expressed (32, 33). Only genes identified by all the 4 methods were considered to be differentially expressed genes. Genes with similar expression shifts (e.g., either up- or down-regulated in the same tissue of the high-altitude species) were selected and then combined. We then performed expression profile analysis of all differentially expressed genes, as described above.

Weighted Gene Coexpression Network Analysis (WGCNA). The gene expression matrix for each tissue was log transformed and used to build a weighted coexpression network using the R package WGCNA (version 1.61) (38) following the guidelines. Briefly, we set different soft thresholds (powers) to fit the scale-free topology and calculate the mean connectivity among genes. We determined a suitable minimum power value to approximate the best scale-free topology using the model fitting index R^2 cut-off. We used 18, 12, 30, 18, and 14 as the best available powers to transform the similarity matrices into adjacency matrices for the lung, cardiac muscle, kidney, liver, and flight muscle, respectively (Fig. S11). We determined a topological overlap measure (TOM) for each pair of genes based on the adjacency matrices. We then performed average linkage hierarchical clustering with TOM-based dissimilarity to construct a dendrogram, setting 0.25 as the height cutoff and 30 as the minimum module size (Fig. S12). We calculated the first principal components as measure of module expressions. We tested the Pearson's correlation between module expression and altitude. We then calculated the Student

asymptotic *P* values for these correlations, correcting for the effects of multiple tests using FDR (32, 33). The modules of highly coexpressed genes with |correlation coefficients| >0.6 and FDR <0.05 were considered altitude-related modules, and genes in these modules were considered to be altitude-associated genes. We then performed expression profile analysis of all altitude-associated genes across all tissues, as described above. We also tested the relationships between module expression and phenotypic traits (body length, body weight, wing length, tail length, tarsus length, and culmen length).

Comparisons of Evolutionary Rates and Detection of Explanatory Variables. We compared the evolutionary rates between differentially expressed genes and nondifferentially expressed genes, and between altitude-associated genes and non-altitude-associated genes. We tested differences in evolutionary rates between complementary gene sets using Mann–Whitney *U* tests. The connectivity of each ortholog was extracted from the WGCNA results for each tissue and then took the average. We then used linear models to determine the effect of altitude, gene expression, and gene connectivity, as well as altitude plus gene expression and altitude plus gene connectivity, on evolutionary rate (dN/dS ratio), using the R package stats (version 3.5.1). Ortholog expression, connectivity, and dN/dS values were log-transformed.

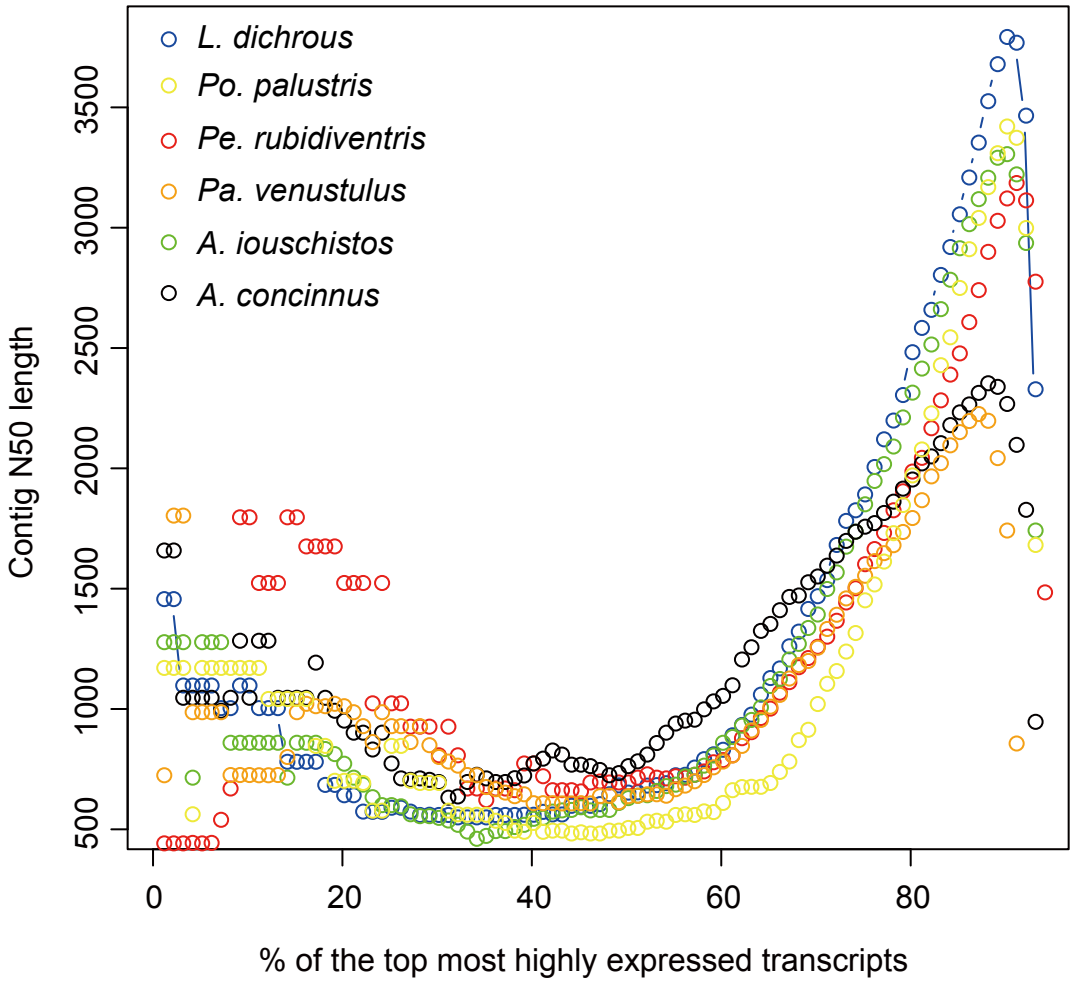

Fig. S1. ExN50 plot of contig N50 length in regard to percentage of the top most highly expressed transcripts.

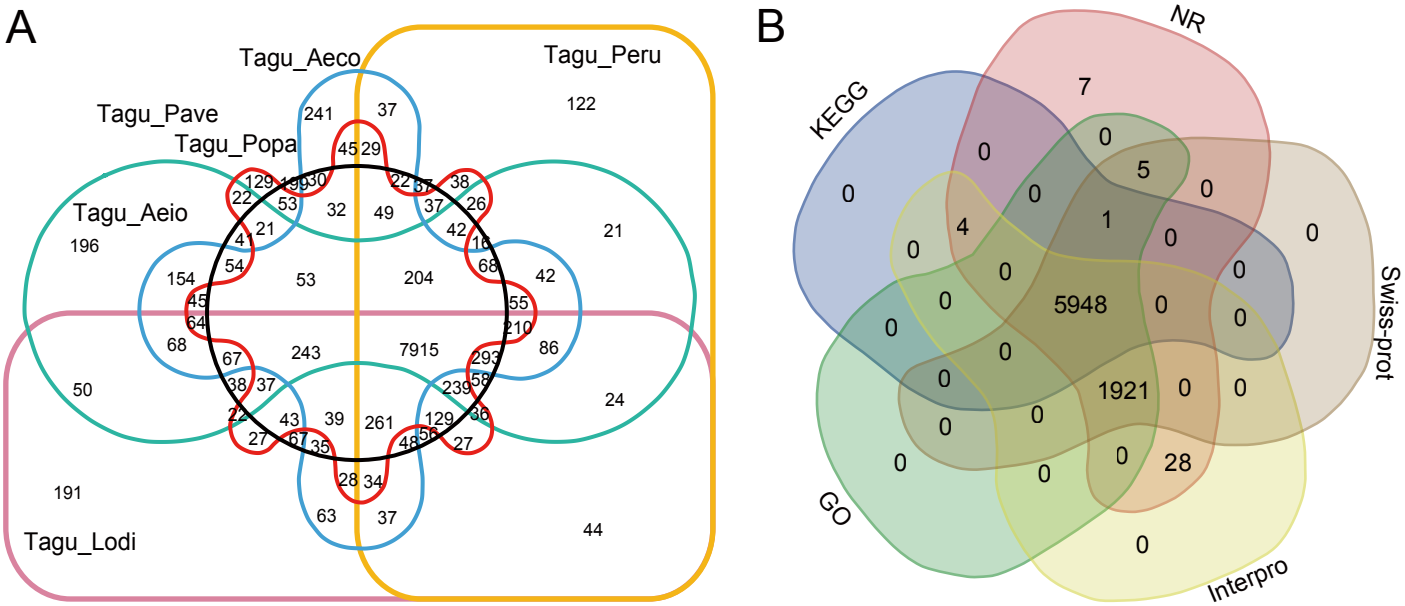

Fig. S2. Venn diagram of (*A*) shared and unique orthologs across the 6 tit species based on the Blast results between these species and *Taeniopygia guttata*, and (*B*) overlapping annotation results of 7,915 orthologs using NR, Swiss-prot, Interpro, GO, and KEGG, produced using TBtools (https://github.com/CJ-Chen/TBtools). Lodi, *Lophophanes dichrous*; Peru, *Periparus rubidiventris*; Aeio, *Aegithalos iouschistos*; Popa, *Poecile palustris*; Pave, *Pardaliparus venustulus*; Aeco, *A. concinnus*; Tagu, *T. guttata*.

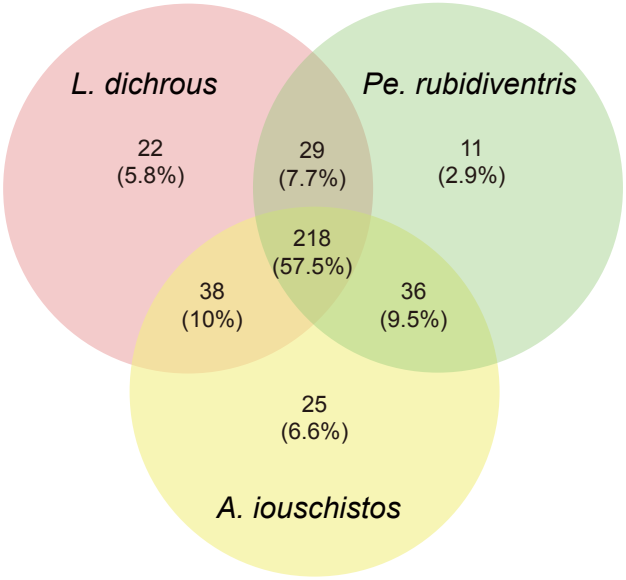

Fig. S3. Venn diagram indicating shared and unique positively selected genes across the 3 high-altitude species. The number and percentage of positively selected genes are shown in the figure.

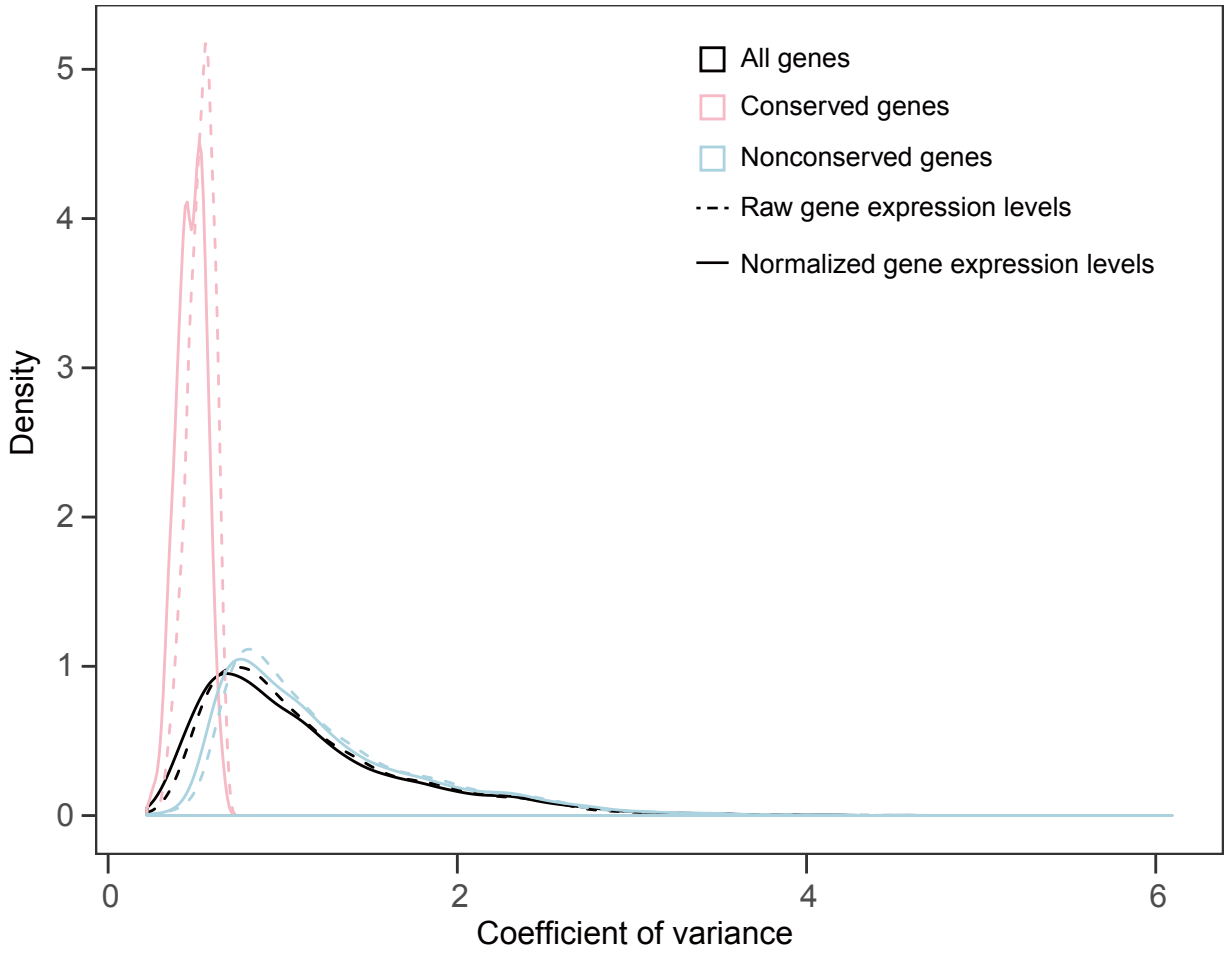

Fig. S4. Distributions of coefficient of variance of gene expression levels among all samples before and after normalization, for all genes, conserved genes, and nonconserved gene.

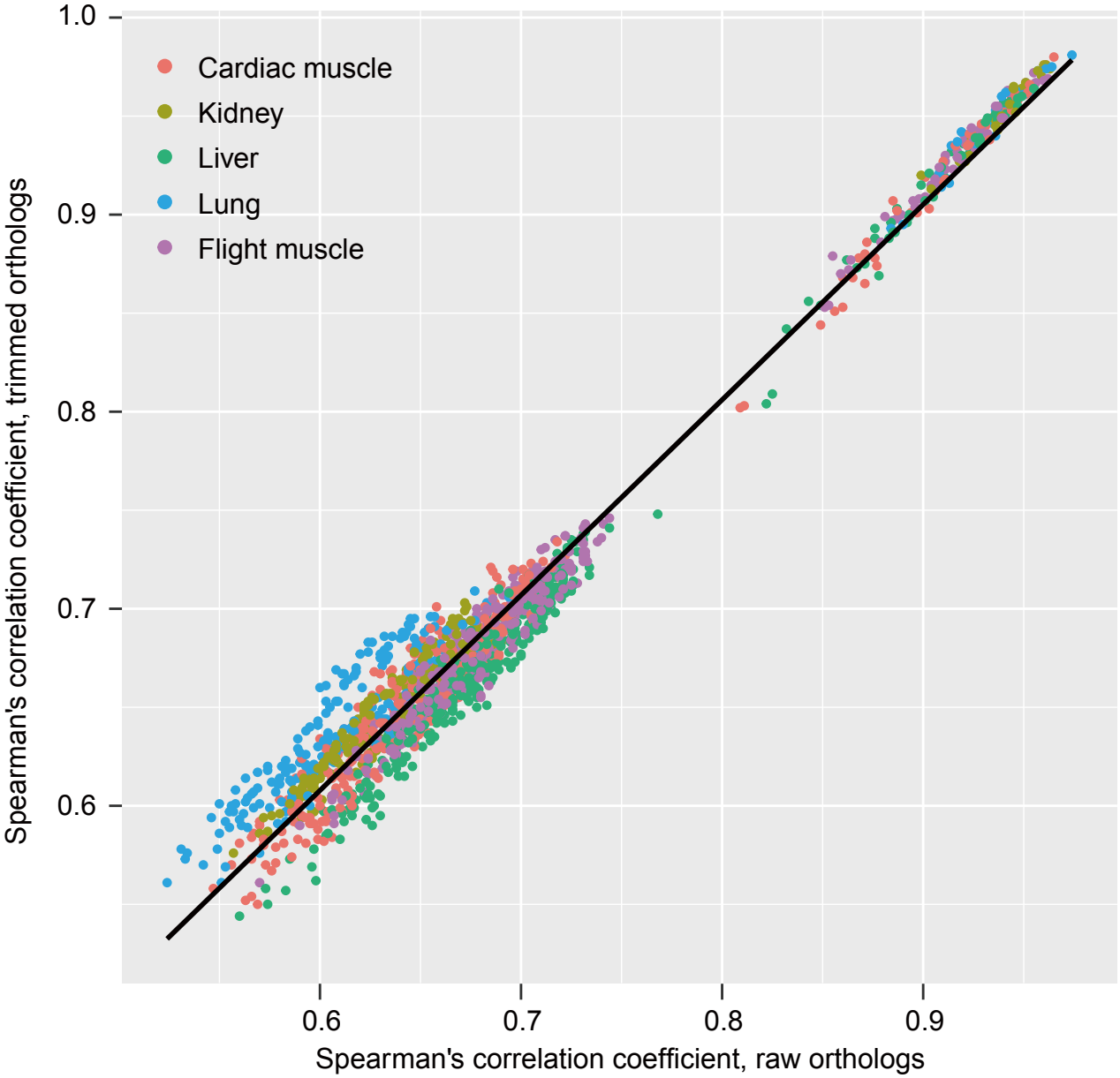

Fig. S5. Comparison of the Spearman's correlation coefficients between all pairs of samples for each tissue based on the gene expression estimations using the trimmed and raw orthologs.

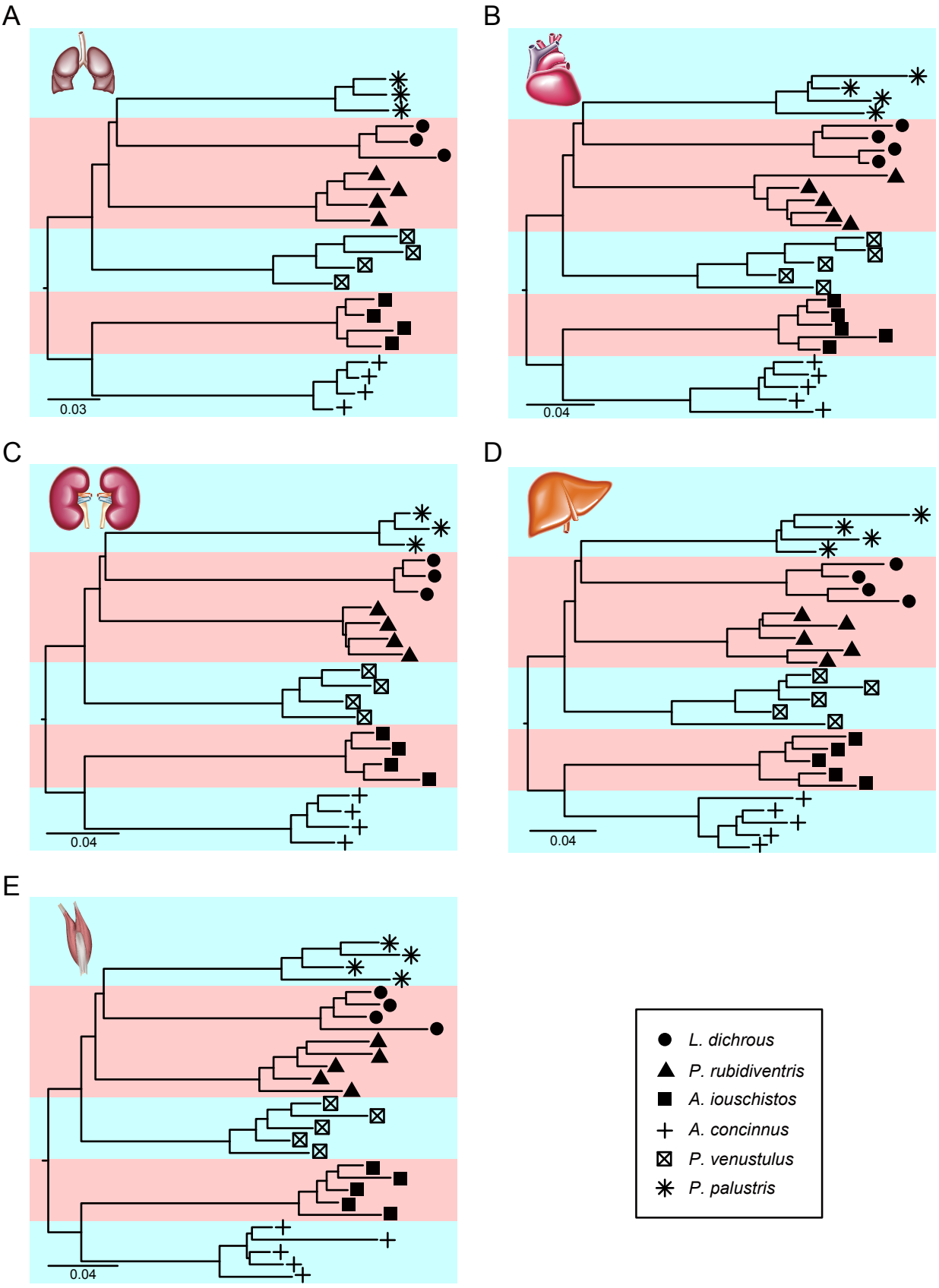

Fig. S6. Neighbour-joining expression trees based on pairwise distance matrices for (*A*) lung, (*B*) cardiac muscle, (*C*) kidney, (*D*) liver, and (*E*) flight muscle.

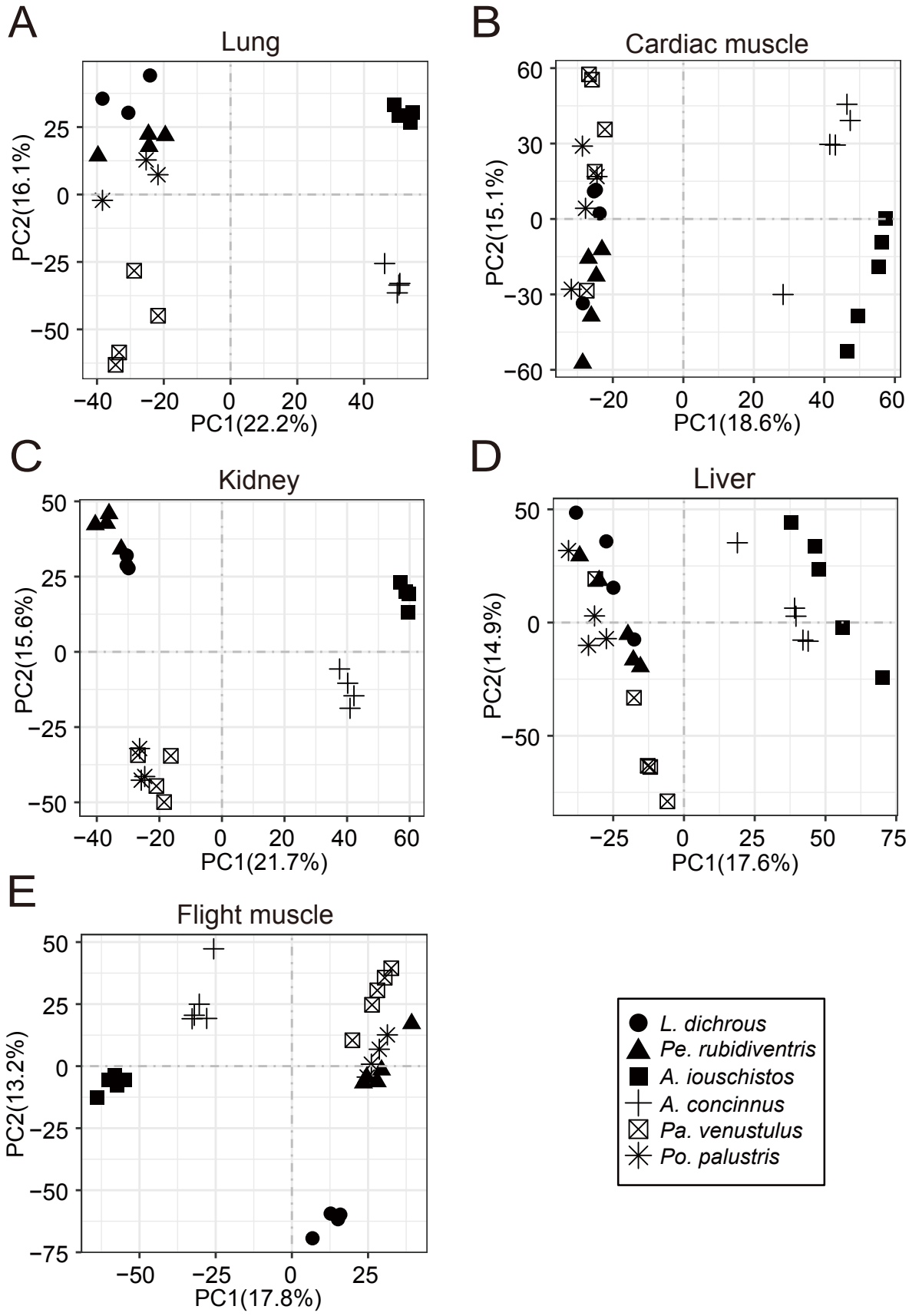

Fig. S7. PCA plot across all species in (*A*) lung, (*B*) cardiac muscle, (*C*) kidney, (*D*) liver, and (*E*) flight muscle. High-altitude species are represented by close symbols, and low-altitude species are represented by open symbols.

A Lung

L. dichrous vs. *Po. palustris*

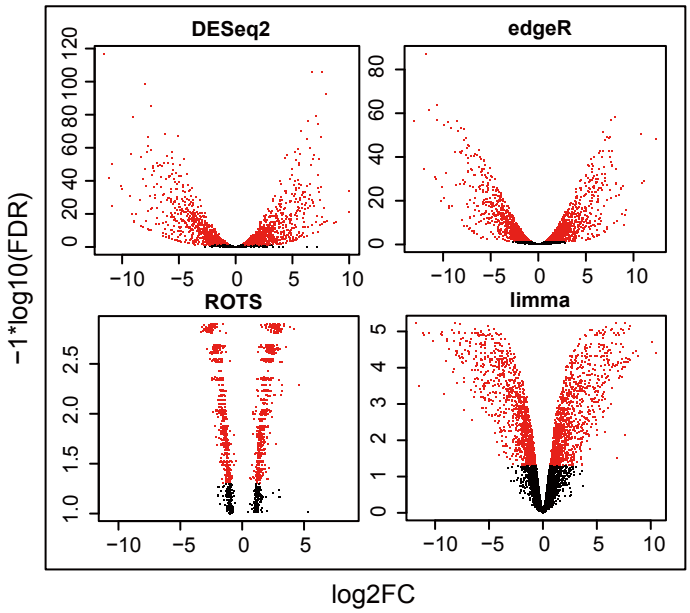

Pe. rubidiventris vs. *Pa. venustulus*

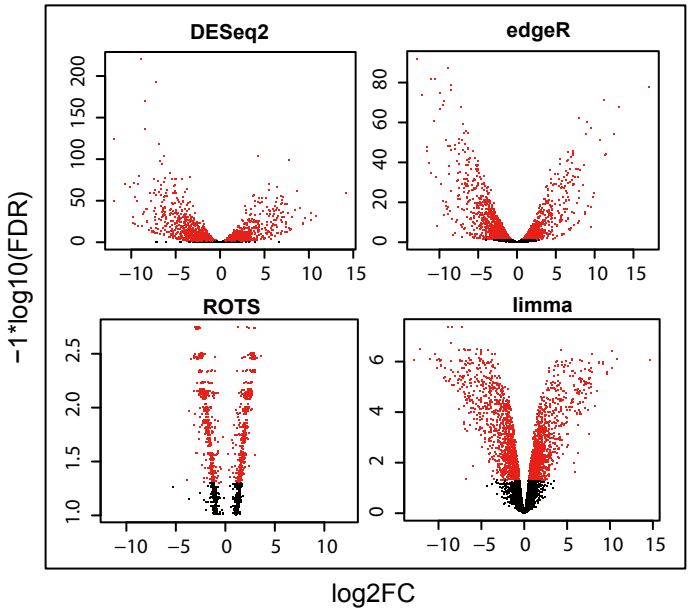

A. iouschistos vs. *A. concinnus*

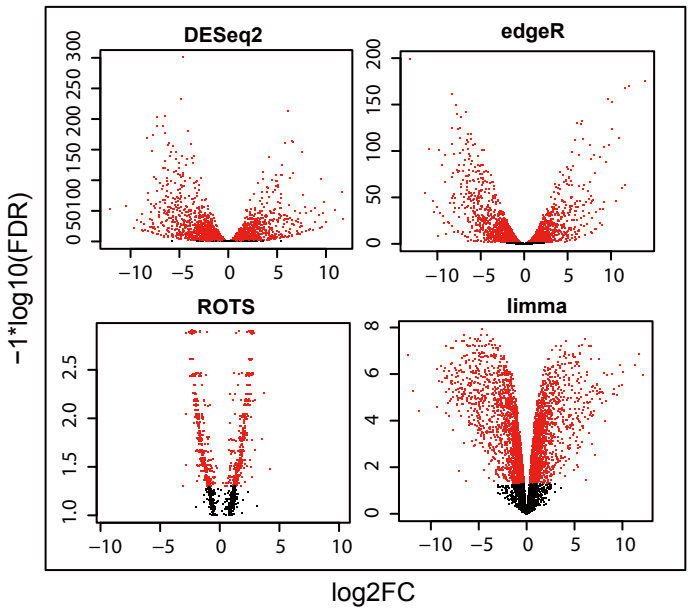

B Cardiac muscle

L. dichrous vs. *Po. palustris*

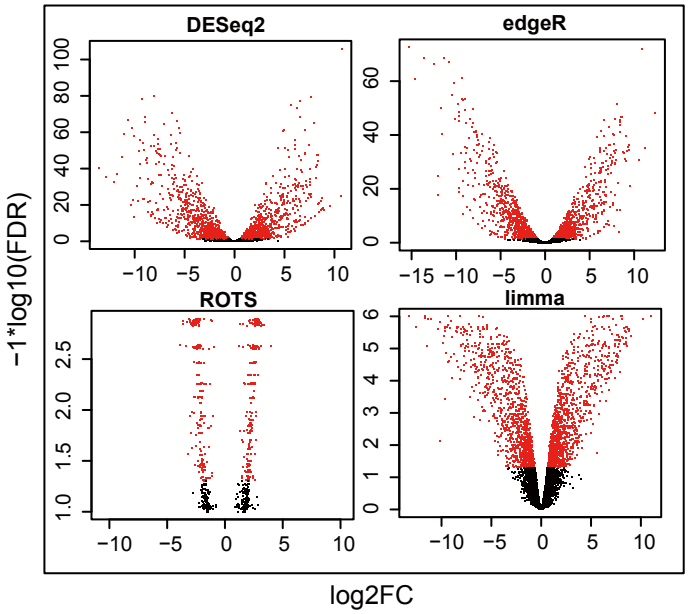

Pe. rubidiventris vs. *Pa. venustulus*

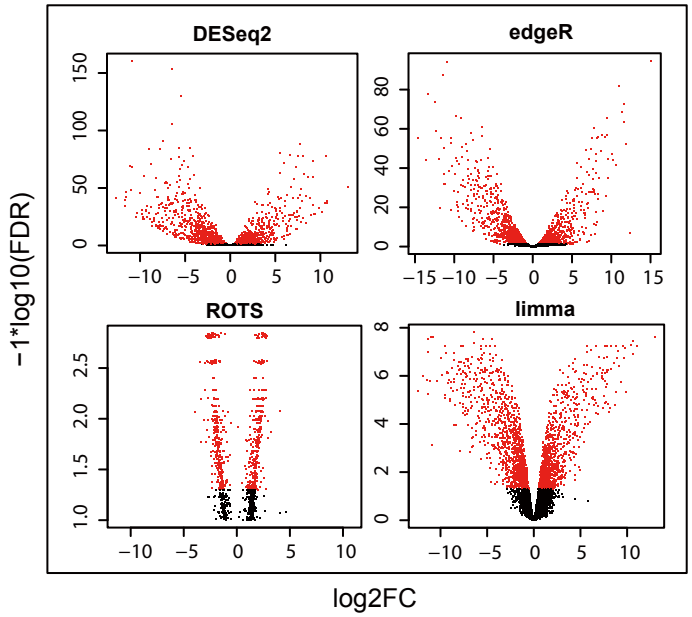

A. iouschistos vs. *A. concinnus*

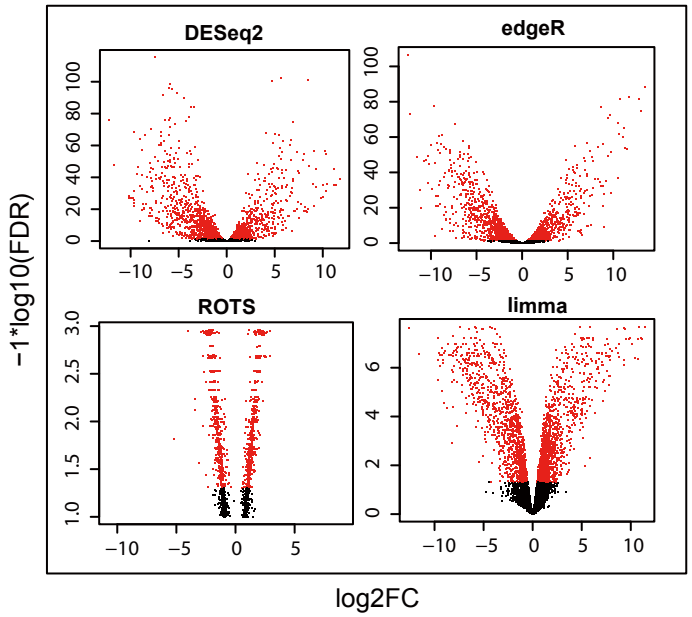

C Kidney

L. dichrous vs. *Po. palustris*

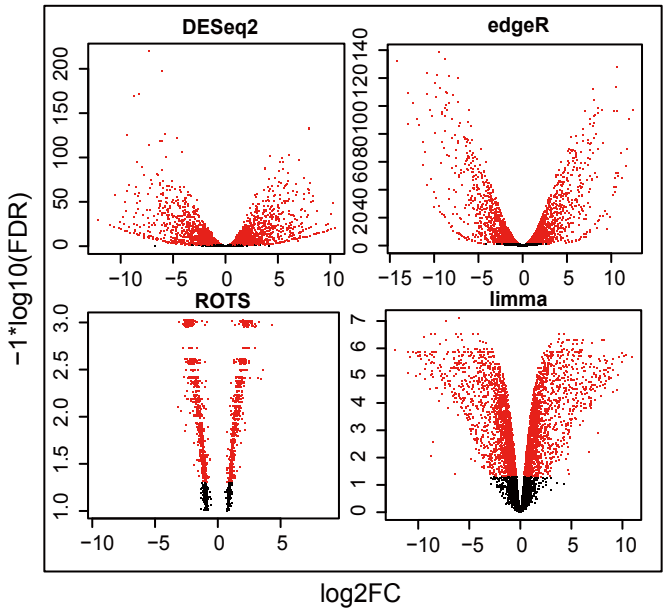

Pe. rubidiventris vs. *Pa. venustulus*

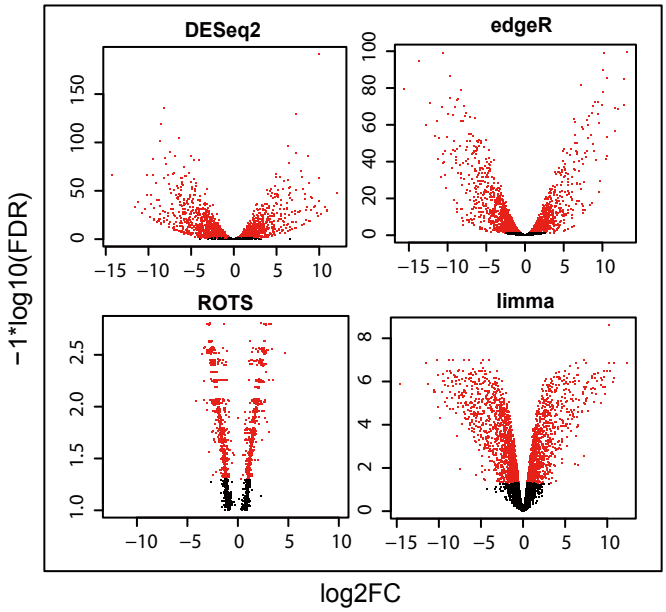

A. iouschistos vs. *A. concinnus*

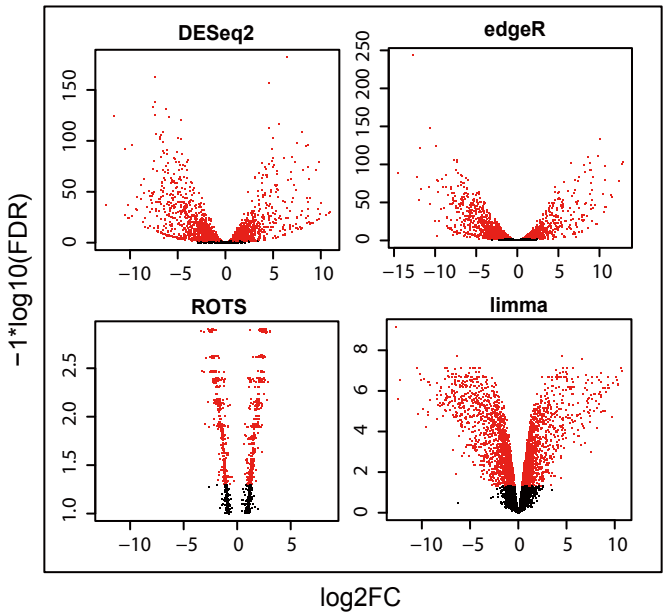

D Liver

L. dichrous vs. *Po. palustris*

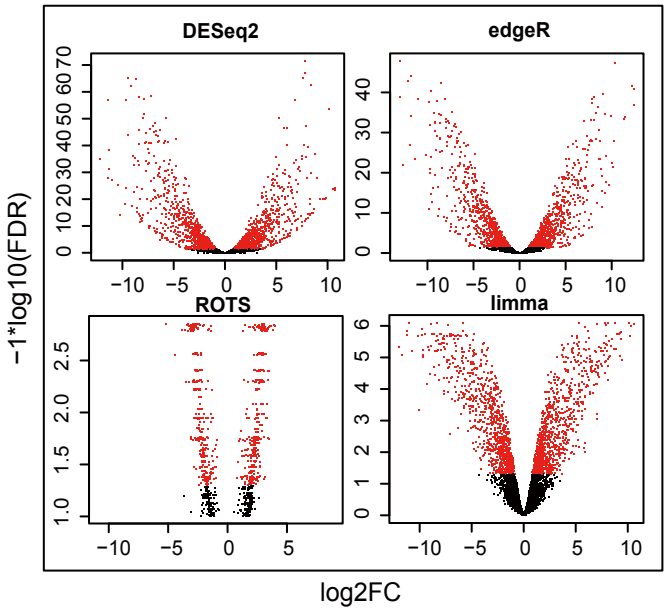

Pe. rubidiventris vs. *Pa. venustulus*

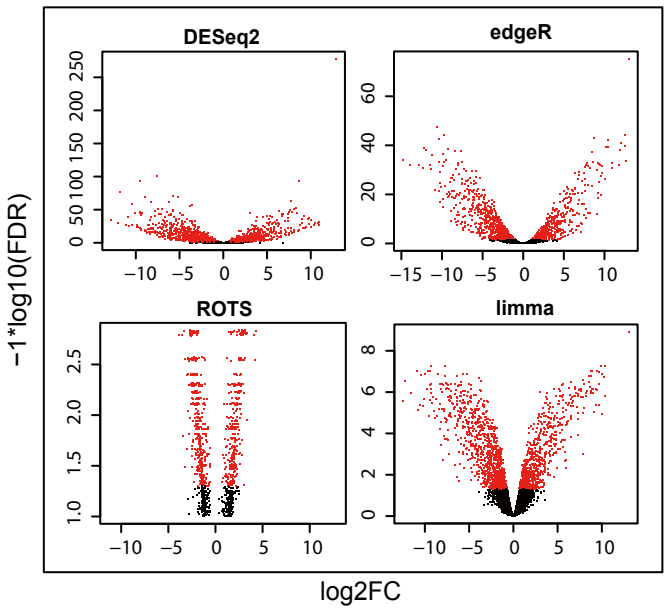

A. iouschistos vs. *A. concinnus*

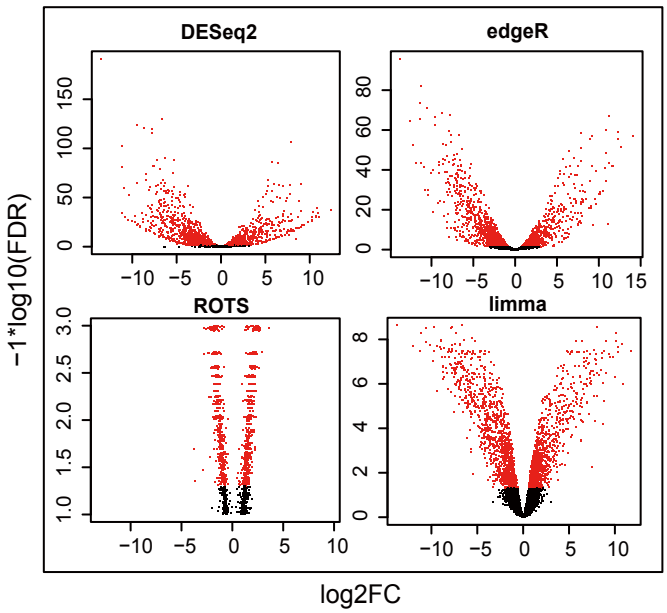

E Flight muscle

L. dichrous vs. *Po. palustris*

Pe. rubidiventris vs. *Pa. venustulus*

A. iouschistos vs. *A. concinnus*

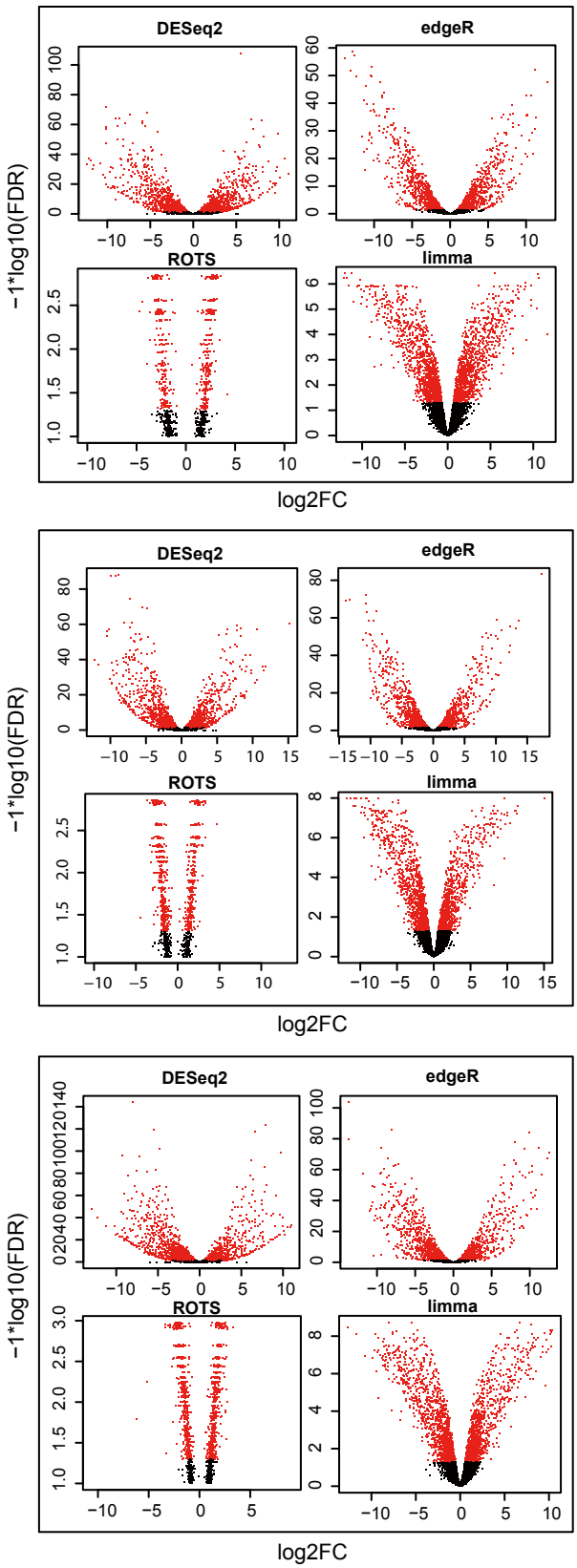

Fig. S8. Volcano plot indicating the results of differential expression analyses using DESeq2, edgeR, ROTS, and limma for genes in (*A*) lung, (*B*) cardiac muscle, (*C*) kidney, (*D*) liver, and (*E*) flight muscle, for the 3 high- and low-altitude pairs. A gene was considered to be a differentially expressed gene if a 2-fold (or greater) expression change between the high- and low-altitude species, and an adjusted *P* value by FDR < 0.05 were observed. Each dot represents one gene. Red dots represent differentially expressed genes. Black dots represent no significantly biased gene.

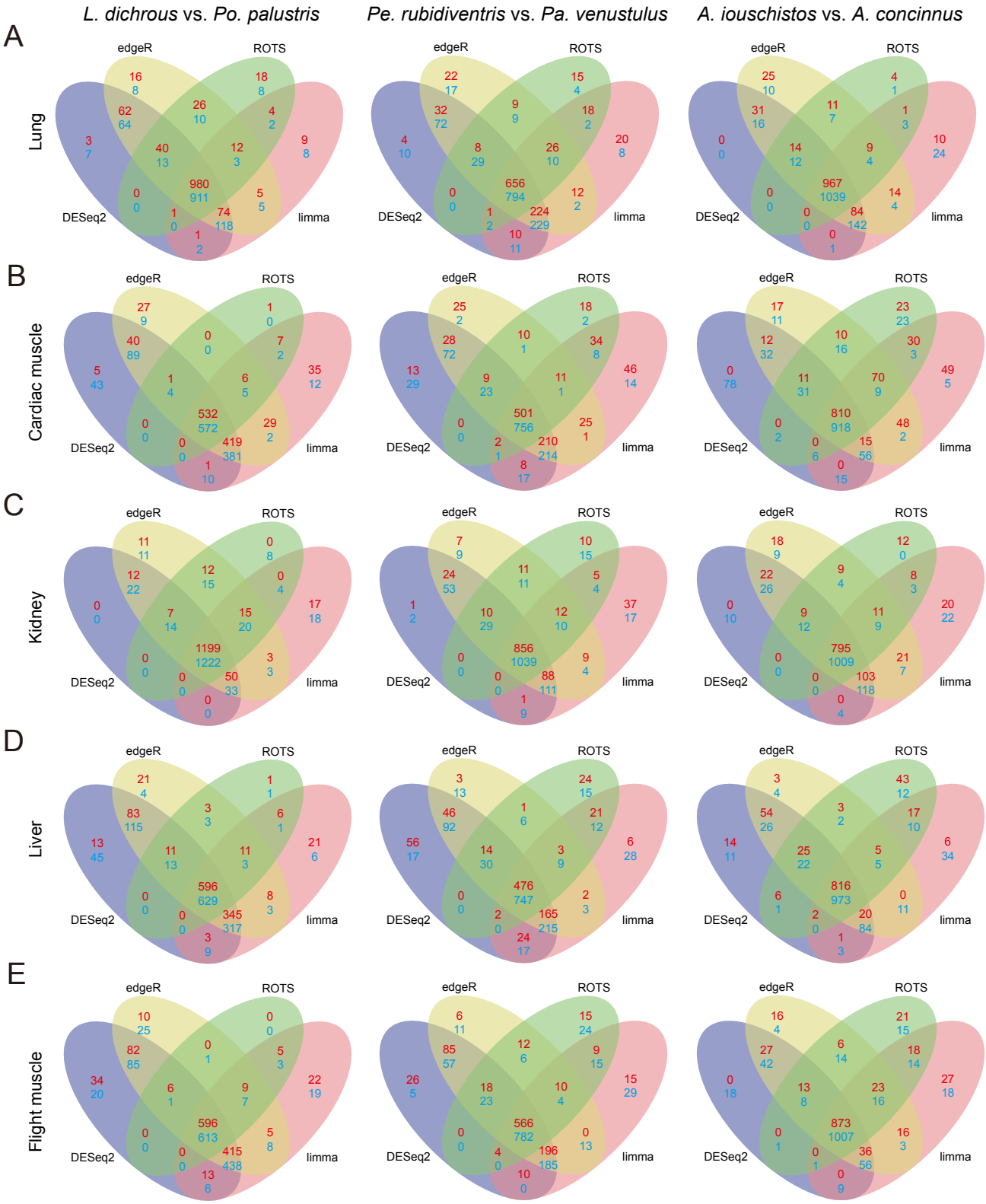

Fig. S9. Venn diagram illustrating differentially expressed genes that were detected by DESeq2, edgeR, ROTS, and limma in (*A*) lung, (*B*) cardiac muscle, (*C*) kidney, (*D*) liver, and (*E*) flight muscle, for the 3 high- and low-altitude pairs. Numbers in red and blue indicate genes up- and down-regulated in the high-altitude species relative to their respective low-altitude species.

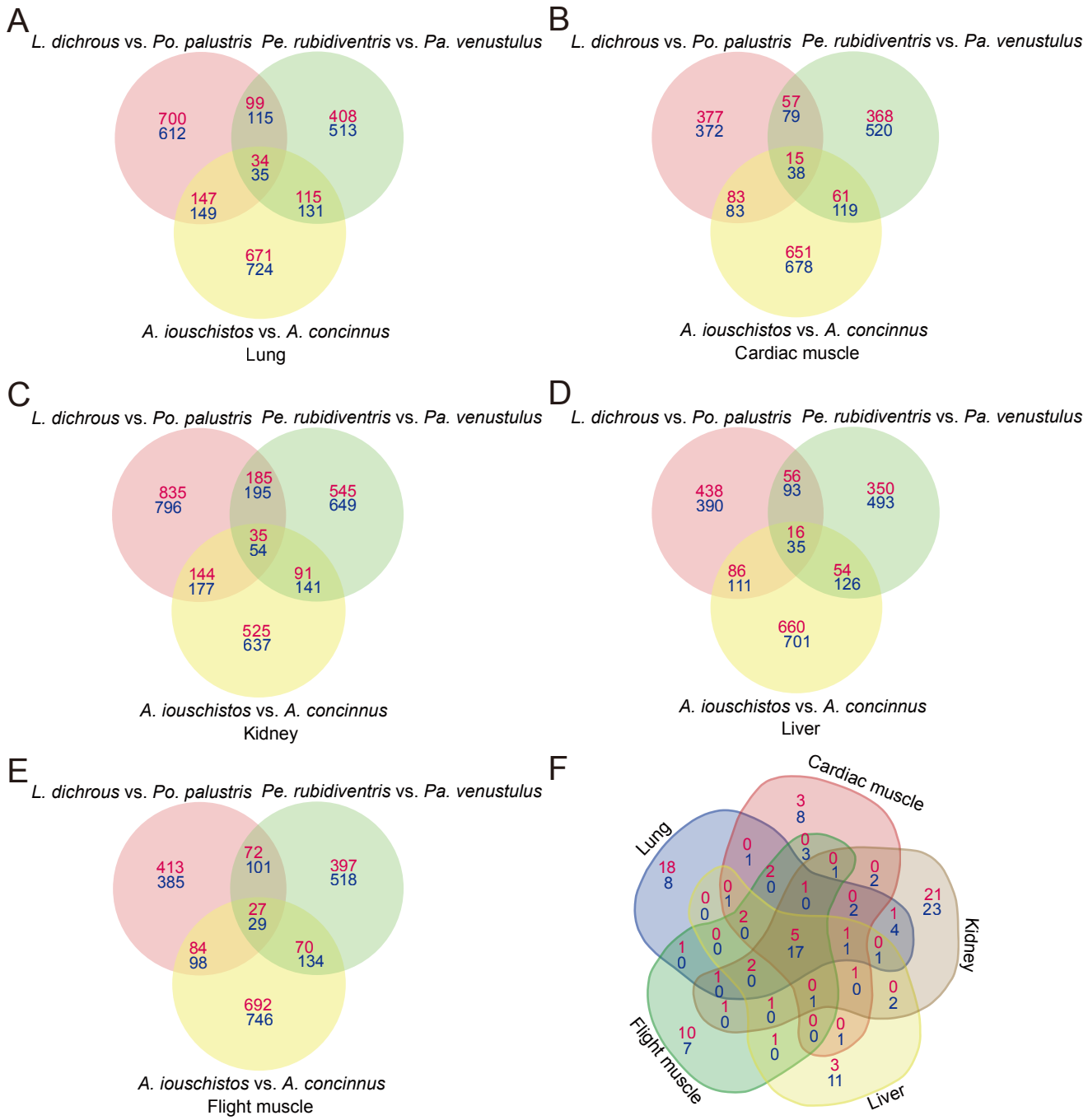

Fig. S10. Venn diagram indicating differentially expressed genes that were shared among the 3 high- and low-altitude pairs in (*A*) lung, (*B*) cardiac muscle, (*C*) kidney, (*D*) liver, and (*E*) flight muscle, and *(F)*. Numbers in red and blue indicate genes up- and down-regulated in the high-altitude species relative to their respective low-altitude species.

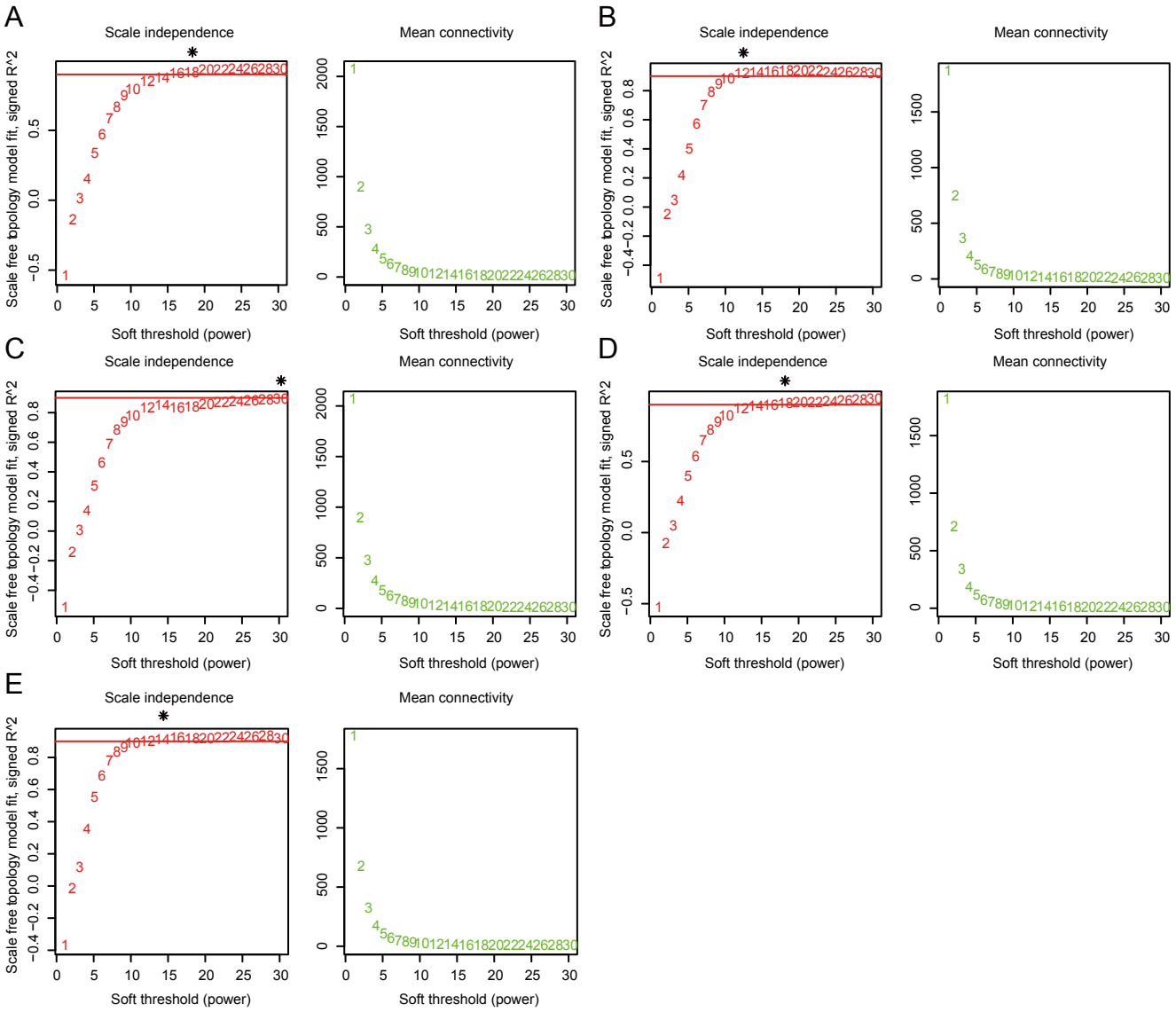

Fig. S11. Plot of scale free topology and mean connectivity in regard to soft-thresholding power for samples from (*A*) lung, (*B*) cardiac muscle, (*C*) kidney, (*D*) liver, and (*E*) flight muscle. Red line indicates an R^2 cut-off of 0.9. Asterisk indicates the soft threshold power chosen for module detection.

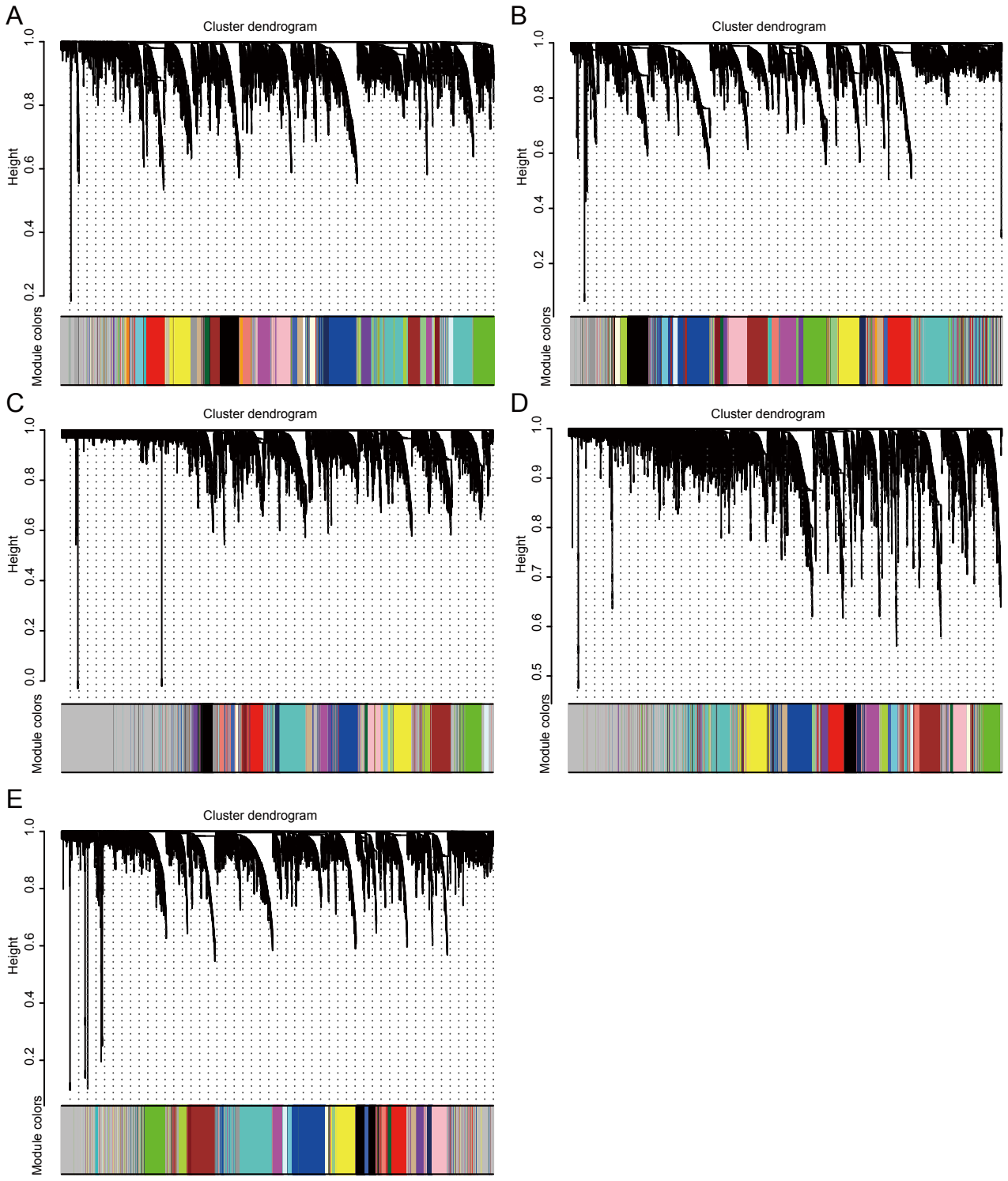

Fig. S12. Clustering dendrogram showing ortholog expression pattern for samples from (*A*) lung, (*B*) cardiac muscle, (*C*) kidney, (*D*) liver, and (*E*) flight muscle. Each colored bar below represents each module.

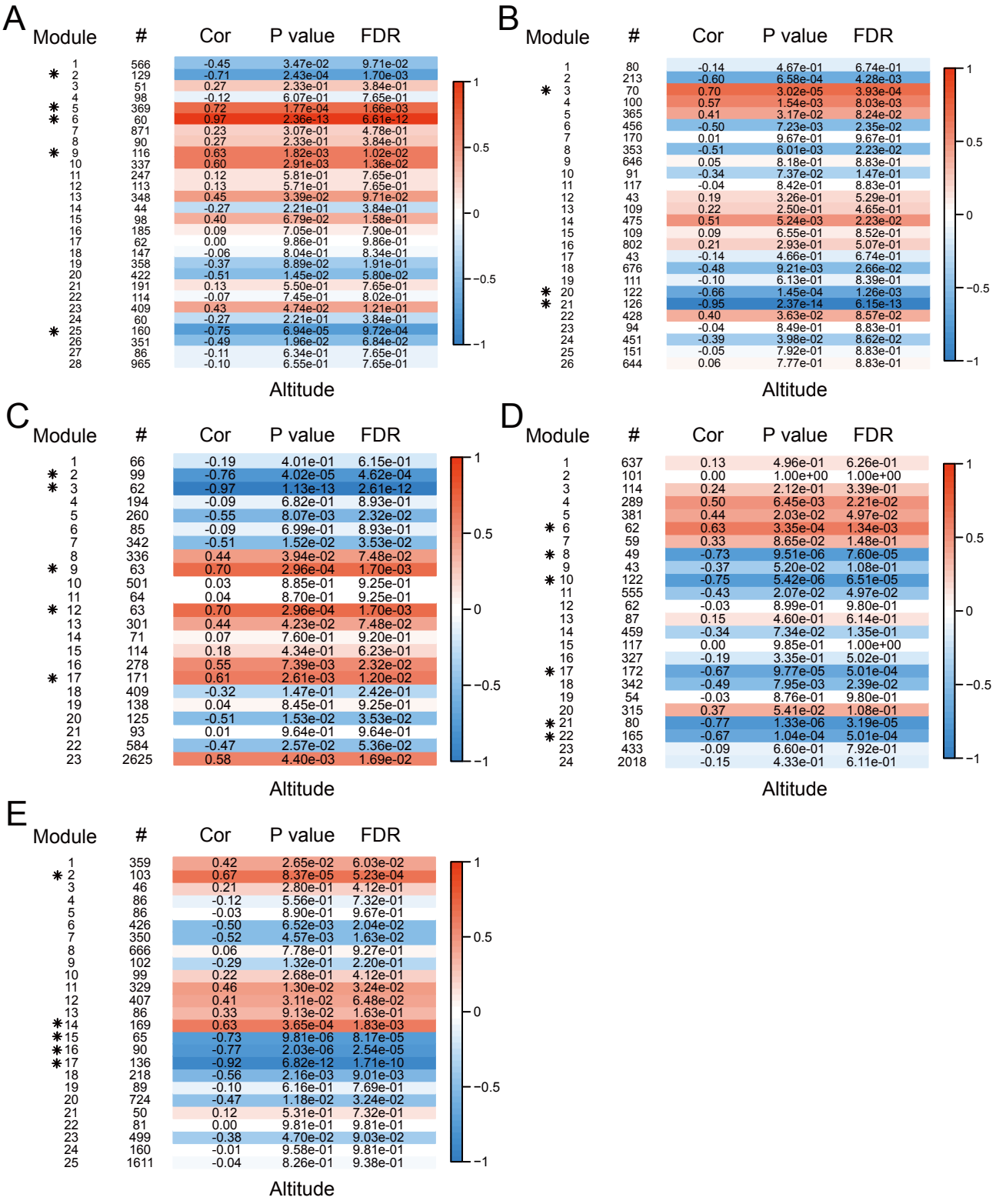

Fig. S13. Pearson's correlation coefficient (Cor) and corresponding significance level (*P* and FDR value) between the expression of each module and the altitude of samples from (*A*) lung, (*B*) cardiac muscle, (*C*) kidney, (*D*) liver, and (*E*) flight muscle. "#" indicates the number of genes in this module. The color bar indicates the correlation coefficient. Asterisk indicates altitude-related module.

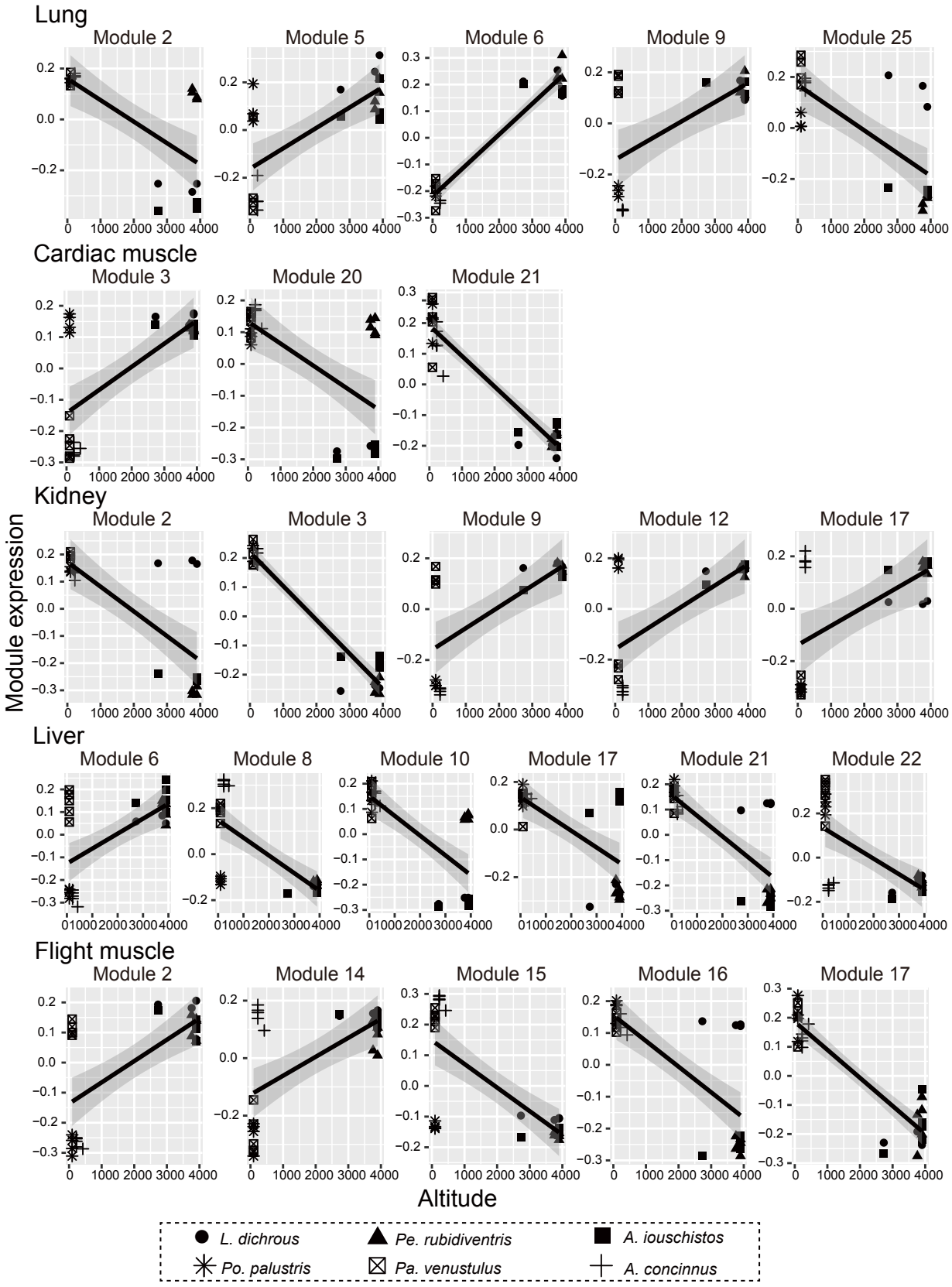

Fig. S14. Graphs showing the significant associations between module expression and altitude for (*A*) lung, (*B*) cardiac muscle, (*C*) kidney, (*D*) liver, and (*E*) flight muscle. Species are represented by point shape.

Table S1. Basic information of the 6 tit species.

Species	Vouch number	Collection site	Sex	Latitude	Longitude	Altitude (m)	Cm	Fm	Lv	Ln	Kd	Sequecing platform
Lophophanes dichrous	HeguM0	Lulang Town, Tibet, China	M	29.65°	94.71°	3,900	√	√	√			Illumina HiSeq 4000
L. dichrous	HeguF1	Yadong County, Tibet, China	F	27.38°	88.97°	2,730	√	√	√	√	√	Illumina HiSeq X Ten
L. dichrous	HeguF2	Yadong County, Tibet, China	F	27.57°	89.03°	3,900	√	√	√	√	√	Illumina HiSeq X Ten
L. dichrous	HeguM1	Yadong County, Tibet, China	M	27.57°	89.00°	3,760	√	√	√	√	√	Illumina HiSeq X Ten
Periparus rubidiventris	HeigM0	Lulang Town, Tibet, China	M	29.65°	94.71°	3,900	√	√	√			Illumina HiSeq 4000
Pe. rubidiventris	HeigF1	Yadong County, Tibet, China	F	27.57°	89.03°	3,900	√	√	√	√	√	Illumina HiSeq X Ten
Pe. rubidiventris	HeigM1	Yadong County, Tibet, China	M	27.57°	89.03°	3,900	√	√	√	√	√	Illumina HiSeq X Ten
Pe. rubidiventris	HeigM2	Yadong County, Tibet, China	M	27.57°	89.00°	3,760	√	√	√	√	√	Illumina HiSeq X Ten
Pe. rubidiventris	HeigM3	Yadong County, Tibet, China	M	27.57°	89.00°	3,760	√	√	√	√	√	Illumina HiSeq X Ten
Aegithalos iouschistos	HetoF0	Lulang Town, Tibet, China	F	29.65°	94.71°	3,900	√	√	√			Illumina HiSeq 4000
A. iouschistos	HetoF1	Yadong County, Tibet, China	F	27.57°	89.03°	3,900	√	√	√	√	√	Illumina HiSeq X Ten
A. iouschistos	HetoF2	Yadong County, Tibet, China	F	27.57°	89.03°	3,900	√	√	√	√	√	Illumina HiSeq X Ten
A. iouschistos	HetoM1	Yadong County, Tibet, China	M	27.57°	89.03°	3,900	√	√	√	√	√	Illumina HiSeq X Ten
A. iouschistos	HetoM2	Yadong County, Tibet, China	M	27.38°	88.97°	2,730	√	√	√	√	√	Illumina HiSeq X Ten
Poecile palustris	ZhzeF0	Huairou District, Beijing, China	F	40.39°	116.66°	95	√	√	√			Illumina HiSeq 4000
Po. palustris	ZhzeF1	Huairou District, Beijing, China	F	40.39°	116.66°	95	√	√	√	√	√	Illumina HiSeq X Ten
Po. palustris	ZhzeF2	Huairou District, Beijing, China	F	40.39°	116.66°	95	√	√	√	√	√	Illumina HiSeq X Ten

Po. palustris	ZhzeM1	Huairou District, Beijing, China	M	40.39°	116.66°	95	√	√	√	√	√	Illumina HiSeq X Ten
Pardaliparus venustulus	HufuM0	Huairou District, Beijing, China	M	40.39°	116.66°	95	√	√	√			Illumina HiSeq 4000
Pa. venustulus	HufuF1	Huairou District, Beijing, China	F	40.39°	116.66°	95	√	√	√	√	√	Illumina HiSeq X Ten
Pa. venustulus	HufuM1	Huairou District, Beijing, China	M	40.39°	116.66°	95	√	√	√	√	√	Illumina HiSeq X Ten
Pa. venustulus	HufuM2	Huairou District, Beijing, China	M	40.39°	116.66°	95	√	√	√	√	√	Illumina HiSeq X Ten
Pa. venustulus	HufuM3	Huairou District, Beijing, China	M	40.39°	116.66°	95	√	√	√	√	√	Illumina HiSeq X Ten
A. concinnus	HotoM0	Jixi County, Anhui, China	M	30.20°	118.53°	423	√	√	√			Illumina HiSeq 4000
A. concinnus	HotoF1	Jixi County, Anhui, China	F	30.08°	118.55°	226	√	√	√	√	√	Illumina HiSeq X Ten
A. concinnus	HotoM1	Jixi County, Anhui, China	M	30.08°	118.55°	226	√	√	√	√	√	Illumina HiSeq X Ten
A. concinnus	HotoM2	Jixi County, Anhui, China	M	30.08°	118.55°	226	√	√	√	√	√	Illumina HiSeq X Ten
A. concinnus	HotoM3	Jixi County, Anhui, China	M	30.08°	118.55°	226	√	√	√	√	√	Illumina HiSeq X Ten

"√" indicates that this tissue was sequenced. Cm, Cardiac muscle; Fm, Flight muscle; Lv, Liver; Ln, Lung; Kd, Kidney; M, Male; F, Female.

Table S2. Basic information of transcriptome sequencing and alignment rates.

Species	Sample name	Clean bases (bp)	Clean Reads	Q20	Q30	GC	Overall mapping rate
L. dichrous	HeguF1_Ln	9,432,901,200	62,886,008	98.73%	95.39%	54.79%	89.80%
L. dichrous	HeguF1_Cm	13,433,093,700	89,553,958	97.16%	92.10%	53.46%	86.07%
L. dichrous	HeguF1_Kd	9,047,755,200	60,318,368	98.40%	94.03%	55.38%	85.71%
L. dichrous	HeguF1_Lv	13,598,628,600	90,657,524	96.59%	91.41%	55.17%	83.33%
L. dichrous	HeguF1_Fm	13,697,594,700	91,317,298	96.25%	90.68%	53.26%	83.04%
L. dichrous	HeguF2_Ln	9,442,329,000	62,948,860	98.71%	95.26%	52.22%	90.81%
L. dichrous	HeguF2_Cm	14,539,201,500	96,928,010	97.23%	92.27%	53.65%	86.07%
L. dichrous	HeguF2_Kd	12,803,231,700	85,354,878	97.77%	93.12%	55.27%	84.46%
L. dichrous	HeguF2_Lv	11,893,043,400	79,286,956	97.65%	92.78%	55.30%	82.38%
L. dichrous	HeguF2_Fm	13,255,542,000	88,370,280	96.35%	90.94%	53.20%	83.05%
L. dichrous	HeguM0_Cm	11,104,946,100	74,032,974	95.18%	88.72%	53.23%	87.01%
L. dichrous	HeguM0_Lv	9,431,719,500	62,878,130	94.95%	88.39%	53.34%	85.11%
L. dichrous	HeguM0_Fm	11,583,836,100	77,225,574	98.12%	94.13%	50.80%	86.37%
L. dichrous	HeguM1_Ln	9,219,009,900	61,460,066	98.66%	95.16%	54.56%	89.43%
L. dichrous	HeguM1_Cm	9,069,689,100	60,464,594	98.50%	94.28%	54.54%	83.88%
L. dichrous	HeguM1_Kd	9,116,568,300	60,777,122	98.41%	94.08%	54.20%	85.90%
L. dichrous	HeguM1_Lv	14,881,887,000	99,212,580	96.39%	90.98%	54.52%	84.49%
L. dichrous	HeguM1_Fm	14,274,740,700	95,164,938	96.22%	90.65%	53.30%	82.55%
Pe. rubidiventris	HeigF1_Ln	9,369,666,000	62,464,440	98.68%	95.17%	53.53%	88.17%
Pe. rubidiventris	HeigF1_Cm	9,711,568,500	64,743,790	96.17%	90.57%	52.44%	87.36%
Pe. rubidiventris	HeigF1_Kd	11,050,219,200	73,668,128	97.90%	93.30%	53.35%	86.33%
Pe. rubidiventris	HeigF1_Lv	13,486,945,800	89,912,972	96.29%	90.80%	55.19%	84.14%
Pe. rubidiventris	HeigF1_Fm	13,071,523,200	87,143,488	97.76%	93.04%	55.00%	82.22%
Pe. rubidiventris	HeigM0_Cm	9,739,182,900	64,927,886	94.95%	88.31%	52.84%	86.21%
Pe. rubidiventris	HeigM0_Lv	9,617,238,600	64,114,924	95.26%	88.99%	54.36%	83.27%
Pe. rubidiventris	HeigM0_Fm	9,490,467,900	63,269,786	95.44%	89.18%	55.14%	82.95%
Pe. rubidiventris	HeigM1_Ln	9,301,864,500	62,012,430	98.64%	95.07%	56.10%	86.86%
Pe. rubidiventris	HeigM1_Cm	10,622,726,400	70,818,176	96.19%	90.58%	53.17%	85.66%
Pe. rubidiventris	HeigM1_Kd	9,138,825,000	60,925,500	98.42%	94.05%	54.63%	86.06%

Pe. rubidiventris	HeigM1_Lv	11,786,049,300	78,573,662	96.53%	91.30%	54.66%	82.31%
Pe. rubidiventris	HeigM1_Fm	12,436,753,500	82,911,690	97.75%	93.01%	55.47%	80.82%
Pe. rubidiventris	HeigM2_Ln	9,366,424,200	62,442,828	98.65%	95.11%	53.58%	87.79%
Pe. rubidiventris	HeigM2_Cm	13,899,282,000	92,661,880	97.03%	91.72%	51.23%	87.36%
Pe. rubidiventris	HeigM2_Kd	9,129,815,100	60,865,434	98.39%	94.03%	54.76%	84.98%
Pe. rubidiventris	HeigM2_Lv	13,204,306,200	88,028,708	96.50%	91.25%	55.57%	82.96%
Pe. rubidiventris	HeigM2_Fm	13,965,715,800	93,104,772	96.04%	90.27%	53.21%	83.90%
Pe. rubidiventris	HeigM3_Ln	9,197,553,000	61,317,020	94.75%	86.99%	52.93%	88.12%
Pe. rubidiventris	HeigM3_Cm	9,084,521,700	60,563,478	94.76%	86.98%	53.91%	86.96%
Pe. rubidiventris	HeigM3_Kd	9,023,647,500	60,157,650	94.88%	87.19%	53.87%	86.41%
Pe. rubidiventris	HeigM3_Lv	9,160,678,800	61,071,192	94.71%	86.88%	55.12%	84.97%
Pe. rubidiventris	HeigM3_Fm	9,034,251,900	60,228,346	94.81%	87.11%	54.72%	84.47%
A. iouschistos	HetoF0_Cm	9,726,937,200	64,846,248	94.91%	88.31%	52.95%	85.47%
A. iouschistos	HetoF0_Lv	9,491,654,700	63,277,698	94.77%	88.10%	54.14%	83.45%
A. iouschistos	HetoF0_Fm	9,630,619,800	64,204,132	95.03%	88.51%	54.15%	84.25%
A. iouschistos	HetoF1_Ln	12,464,010,300	83,093,402	97.94%	93.52%	53.88%	87.59%
A. iouschistos	HetoF1_Cm	10,558,803,600	70,392,024	96.39%	90.92%	52.69%	85.96%
A. iouschistos	HetoF1_Kd	9,187,362,900	61,249,086	98.78%	95.12%	54.11%	85.88%
A. iouschistos	HetoF1_Lv	13,882,547,700	92,550,318	96.28%	90.80%	54.43%	84.73%
A. iouschistos	HetoF1_Fm	12,082,806,600	80,552,044	96.17%	90.55%	52.30%	84.40%
A. iouschistos	HetoF2_Ln	12,974,160,900	86,494,406	97.51%	92.79%	55.33%	85.87%
A. iouschistos	HetoF2_Cm	10,544,150,400	70,294,336	96.38%	90.94%	53.79%	85.13%
A. iouschistos	HetoF2_Kd	11,849,843,700	78,998,958	97.99%	93.51%	52.24%	87.12%
A. iouschistos	HetoF2_Lv	12,675,019,500	84,500,130	96.43%	91.09%	55.14%	84.47%
A. iouschistos	HetoF2_Fm	13,064,605,800	87,097,372	96.08%	90.37%	52.78%	83.88%
A. iouschistos	HetoM1_Ln	11,910,697,200	79,404,648	97.87%	93.36%	53.61%	87.75%
A. iouschistos	HetoM1_Cm	14,656,521,900	97,710,146	97.13%	91.89%	51.38%	86.14%
A. iouschistos	HetoM1_Kd	12,768,854,700	85,125,698	97.75%	93.14%	53.30%	86.25%
A. iouschistos	HetoM1_Lv	11,769,827,400	78,465,516	97.40%	92.30%	55.71%	83.34%
A. iouschistos	HetoM1_Fm	15,275,615,400	101,837,436	96.03%	90.26%	52.56%	83.64%
A. iouschistos	HetoM2_Ln	9,162,181,800	61,081,212	98.64%	95.10%	54.70%	87.15%
A. iouschistos	HetoM2_Cm	9,345,440,100	62,302,934	96.37%	90.91%	53.70%	84.24%

A. iouschistos	HetoM2_Kd	11,880,356,400	79,202,376	97.90%	93.41%	52.86%	86.08%
A. iouschistos	HetoM2_Lv	11,668,041,600	77,786,944	96.24%	90.70%	54.13%	84.69%
A. iouschistos	HetoM2_Fm	15,814,523,100	105,430,154	95.87%	89.92%	52.54%	83.93%
A. concinnus	HotoF1_Ln	9,469,968,300	63,133,122	98.70%	95.24%	53.37%	84.59%
A. concinnus	HotoF1_Cm	12,709,832,400	84,732,216	96.18%	90.71%	54.27%	82.36%
A. concinnus	HotoF1_Kd	9,046,133,400	60,307,556	98.69%	94.98%	52.54%	84.96%
A. concinnus	HotoF1_Lv	9,062,352,900	60,415,686	98.53%	94.27%	53.68%	82.70%
A. concinnus	HotoF1_Fm	14,262,681,900	95,084,546	96.96%	91.65%	51.75%	83.80%
A. concinnus	HotoM0_Cm	9,331,496,100	62,209,974	95.06%	88.57%	52.23%	84.19%
A. concinnus	HotoM0_Lv	9,128,928,900	60,859,526	95.10%	88.67%	53.67%	83.22%
A. concinnus	HotoM0_Fm	9,659,484,300	64,396,562	95.15%	88.71%	54.06%	81.87%
A. concinnus	HotoM1_Ln	9,409,670,100	62,731,134	98.66%	95.13%	53.95%	84.96%
A. concinnus	HotoM1_Cm	14,904,018,000	99,360,120	97.06%	91.90%	53.88%	82.79%
A. concinnus	HotoM1_Kd	9,067,175,400	60,447,836	98.36%	93.87%	54.22%	84.44%
A. concinnus	HotoM1_Lv	9,031,335,000	60,208,900	98.62%	94.70%	55.27%	83.24%
A. concinnus	HotoM1_Fm	9,223,153,500	61,487,690	98.68%	95.10%	51.22%	84.70%
A. concinnus	HotoM2_Ln	9,449,225,400	62,994,836	98.70%	95.25%	53.44%	84.70%
A. concinnus	HotoM2_Cm	9,159,245,100	61,061,634	96.31%	90.80%	55.59%	82.40%
A. concinnus	HotoM2_Kd	12,031,299,000	80,208,660	97.88%	93.26%	53.33%	85.13%
A. concinnus	HotoM2_Lv	11,741,631,900	78,277,546	97.90%	93.45%	55.58%	82.63%
A. concinnus	HotoM2_Fm	10,054,312,500	67,028,750	96.17%	90.46%	52.84%	83.13%
A. concinnus	HotoM3_Ln	11,982,162,900	79,881,086	97.30%	92.39%	53.69%	83.99%
A. concinnus	HotoM3_Cm	11,872,052,700	79,147,018	97.42%	92.66%	52.83%	84.20%
A. concinnus	HotoM3_Kd	11,316,913,800	75,446,092	98.04%	93.64%	51.81%	85.94%
A. concinnus	HotoM3_Lv	12,331,863,600	82,212,424	97.59%	92.77%	53.92%	80.66%
A. concinnus	HotoM3_Fm	12,050,244,300	80,334,962	97.74%	92.98%	54.38%	80.85%
Pa. venustulus	HufuF1_Ln	11,468,901,600	76,459,344	98.13%	94.16%	54.44%	83.30%
Pa. venustulus	HufuF1_Cm	14,386,120,800	95,907,472	97.06%	91.96%	53.79%	84.97%
Pa. venustulus	HufuF1_Kd	9,209,953,800	61,399,692	98.77%	95.31%	54.76%	84.33%
Pa. venustulus	HufuF1_Lv	12,062,974,200	80,419,828	97.58%	92.85%	54.73%	82.22%
Pa. venustulus	HufuF1_Fm	10,324,471,800	68,829,812	96.19%	90.50%	54.29%	84.50%
Pa. venustulus	HufuM0_Cm	8,554,963,200	57,033,088	95.07%	88.57%	52.84%	84.84%

Pa. venustulus	HufuM0_Lv	10,115,175,900	67,434,506	95.84%	89.64%	52.54%	83.75%
Pa. venustulus	HufuM0_Fm	8,425,998,600	56,173,324	95.06%	88.51%	55.33%	83.23%
Pa. venustulus	HufuM1_Ln	9,351,926,400	62,346,176	98.51%	94.75%	57.43%	85.69%
Pa. venustulus	HufuM1_Cm	9,971,352,600	66,475,684	96.38%	90.97%	55.06%	84.64%
Pa. venustulus	HufuM1_Kd	9,053,757,300	60,358,382	98.73%	95.15%	54.07%	84.36%
Pa. venustulus	HufuM1_Lv	12,427,436,100	82,849,574	97.83%	93.32%	56.14%	80.56%
Pa. venustulus	HufuM1_Fm	10,980,888,900	73,205,926	97.69%	92.90%	55.31%	81.34%
Pa. venustulus	HufuM2_Ln	10,825,193,700	72,167,958	98.17%	94.25%	56.41%	84.87%
Pa. venustulus	HufuM2_Cm	14,060,781,300	93,738,542	97.29%	92.32%	54.96%	85.63%
Pa. venustulus	HufuM2_Kd	11,382,315,600	75,882,104	97.97%	93.76%	51.54%	86.32%
Pa. venustulus	HufuM2_Lv	12,396,849,300	82,645,662	97.85%	93.29%	55.93%	81.34%
Pa. venustulus	HufuM2_Fm	9,407,762,700	62,718,418	96.37%	90.88%	54.57%	83.97%
Pa. venustulus	HufuM3_Ln	9,364,850,400	62,432,336	98.71%	95.29%	53.65%	84.19%
Pa. venustulus	HufuM3_Cm	13,937,123,100	92,914,154	97.41%	92.55%	53.68%	85.31%
Pa. venustulus	HufuM3_Kd	9,192,838,200	61,285,588	98.49%	94.24%	53.85%	85.83%
Pa. venustulus	HufuM3_Lv	11,538,076,800	76,920,512	97.66%	93.01%	56.78%	81.22%
Pa. venustulus	HufuM3_Fm	11,708,659,500	78,057,730	96.43%	91.06%	54.87%	83.65%
Po. palustris	ZhzeF0_Cm	9,444,469,200	62,963,128	94.14%	86.27%	53.28%	85.31%
Po. palustris	ZhzeF0_Lv	10,961,786,400	73,078,576	94.58%	87.81%	52.60%	84.63%
Po. palustris	ZhzeF0_Fm	8,594,658,000	57,297,720	94.74%	87.70%	54.81%	83.43%
Po. palustris	ZhzeF1_Ln	9,344,865,900	62,299,106	98.60%	94.97%	53.54%	89.73%
Po. palustris	ZhzeF1_Cm	13,167,495,000	87,783,300	97.45%	92.62%	55.29%	84.10%
Po. palustris	ZhzeF1_Kd	9,136,260,600	60,908,404	98.43%	94.10%	53.21%	84.92%
Po. palustris	ZhzeF1_Lv	13,758,102,600	91,720,684	96.33%	91.06%	54.61%	82.15%
Po. palustris	ZhzeF1_Fm	13,363,463,100	89,089,754	96.19%	90.53%	53.28%	81.70%
Po. palustris	ZhzeF2_Ln	9,323,894,700	62,159,298	98.62%	94.99%	53.39%	90.06%
Po. palustris	ZhzeF2_Cm	13,845,483,600	92,303,224	97.28%	92.31%	54.37%	84.19%
Po. palustris	ZhzeF2_Kd	9,064,197,000	60,427,980	98.49%	94.27%	52.34%	86.41%
Po. palustris	ZhzeF2_Lv	16,986,259,800	113,241,732	96.31%	91.14%	53.95%	78.75%
Po. palustris	ZhzeF2_Fm	13,511,502,900	90,076,686	96.02%	90.21%	53.34%	82.28%
Po. palustris	ZhzeM1_Ln	9,389,426,400	62,596,176	98.60%	94.96%	57.09%	88.87%
Po. palustris	ZhzeM1_Cm	12,918,468,900	86,123,126	97.38%	92.48%	53.82%	85.35%

Po. palustris	ZhzeM1_Kd	9,177,409,500	61,182,730	98.51%	94.35%	52.78%	86.30%
Po. palustris	ZhzeM1_Lv	14,497,727,100	96,651,514	96.13%	90.67%	53.20%	81.66%
Po. palustris	ZhzeM1_Fm	13,927,655,400	92,851,036	96.08%	90.29%	52.93%	83.14%

Cm, Cardiac muscle; Fm, Flight muscle; Lv, Liver; Ln, Lung; Kd, Kidney.

Table S3. Basic information of de novo transcriptome assembly using Trinity and CD-HIT.

Species	Contig ExN50 peak length	Number of transcripts
L. dichrous	3,790	27,581
Po. palustris	3,418	28,909
Pe. rubidiventris	3,183	31,493
Pa. venustulus	2,223	30,074
A. iouschistos	3,303	36,505
A. concinnus	2,351	28,412

Table S4. Statistics of BUSCO for the transcriptome assembly quality assessment of the 6 tit species.

	L. dichrous	*Pe. rubidiventris*	*A. iouschistos*	*A. concinnus*	*Pa. venustulus*	*Po. palustris*
Complete BUSCOs	3,958 (80.5%)	3,795 (77.2%)	3,760 (76.5%)	3,691 (75.1%)	3,572 (72.7%)	3,917 (79.7%)
Fragmented BUSCOs	509 (10.4%)	608 (12.4%)	629 (12.8%)	702 (14.3%)	772 (15.7%)	510 (10.4%)
Missing BUSCOs	448 (9.1%)	512 (10.4%)	526 (10.7%)	522 (10.6%)	571 (11.6%)	488 (9.9%)
Total BUSCO groups searched	4,915 (100%)	4,915 (100%)	4,915 (100%)	4,915 (100%)	4,915 (100%)	4,915 (100%)

Note that complete BUSCOs include single-copy and duplicate BUSCOs. Percentages of the total number of BUSCO groups searched are shown in parentheses (bottom).

Table S5. Branch-site likelihood ratio tests and the corresponding number of positively selected genes.

Test No.	High-altitude species as foreground branch	No. of positively selected genes
1	*L. dichrous*	81
2	*L. dichrous* and *Pe. rubidiventris*	151
3	*L. dichrous*, *Pe. Rubidiventris*, and *A. iouschistos*	203
4	*L. dichrous* and *A. iouschistos*	154
5	*Pe. rubidiventris*	77
6	*Pe. rubidiventris* and *A. iouschistos*	149
7	*A. iouschistos*	99
Total	~	379

Table S6. Three different strategies used in convergence analysis of the high-altitude species and the corresponding number of convergent genes.

Strategy No.	Convergence in high-altitude species	No. of convergent genes
1	*L. dichrous* and *Pe. rubidiventris*	143
2	*L. dichrous* and *A. iouschistos*	86
3	*Pe. rubidiventris* and *A. iouschistos*	68
Total	~	280

Table S7. Adaptively convergent genes identified under positive selection with nonsynonymous convergent amino acid changes.

Gene	Branch along which positive selection was detected (*P* value)	Species in which convergence was detected (*P* value)	Convergent amino acid substitution
HOOK3	Lodi, Peru, Aeio (0.0048); Lodi, Peru (0.0076); Lodi, Aeio (0.0017); Lodi (0.0017)	Lodi, Aeio (0.0051)	N24D
CYP8B1	Lodi, Aeio (0.0323)	Lodi, Aeio (0.0024)	I125A, F171Y, H278Y
		Peru, Aeio (0.0314)	Q191R, I331V
SAFB1	Lodi, Peru, Aeio (0.0223); Lodi, Aeio (0.0145)	Lodi, Aeio (0.0144)	I551V
IFNAR2	Lodi, Peru, Aeio (0.0039); Lodi, Aeio (0.0199); Lodi (0.0379)	Lodi, Peru (0.0012)	S15G, R61Q
		Lodi, Aeio (0.0209)	R61Q
		Peru, Aeio (0.0134)	R61Q
G3BP1	Lodi, Peru, Aeio (<0.0001)*; Lodi, Peru (<0.0001)*	Lodi, Peru (0.0018)	S361K, Y362L
CEP85	Lodi, Peru (0.0198)	Lodi, Peru (0.0048)	T280S
DYRK3	Lodi, Peru (0.0439)	Lodi, Peru (0.003)	T24A
NEBL	Peru, Aeio (0.0148)	Peru, Aeio (0.0031)	V639I
KIAA1328	Lodi, Peru, Aeio (0.0034); Lodi, Peru (0.0003)*; Lodi, Aeio (0.0130); Lodi (0.0008)	Lodi, Peru (0.0327)	G50S
GOGA4	Lodi, Aeio (0.0074); Aeio (0.0002)*	Lodi, Peru (0.0081)	S2041N
FRITZ	Lodi, Peru (0.0357)	Lodi, Peru (0.0067)	G190C
K2013	Lodi, Aeio (0.0420)	Lodi, Aeio (0.0029)	S51T
MCFD2	Peru, Aeio (0.0179)	Peru, Aeio (0.0005)	R124K, S130N
TNR27	Lodi, Peru (0.0320)	Lodi, Peru (0.0042)	P238L
CBX3	Lodi, Peru, Aeio (<0.0001)*; Lodi, Peru (<0.0001)*	Lodi, Peru (0.0034)	T7I, L8E
COG1	Lodi, Peru (0.0139)	Lodi, Peru (0.0035)	A424V
HN1L	Lodi, Peru, Aeio (0.0006)*	Lodi, Peru (0.0032)	Q153R
		Lodi, Aeio (0.0027)	Q153R
		Peru, Aeio (0.0013)	Q153R
DJC12	Lodi, Peru, Aeio (0.0042); Lodi, Peru (0.0042)	Lodi, Peru (0.0015)	S107G, G119D
YKT6	Lodi, Peru, Aeio (0.0190); Lodi, Aeio (0.0190)	Lodi, Aeio (0.0058)	Q104E
GAB3	Lodi, Peru, Aeio (0.0493); Lodi, Peru (0.0137)	Lodi, Peru (0.0019)	G489S

AGGF1	Lodi, Peru (0.0482)	Lodi, Peru (0.0031)	S107L
LOC101233820	Peru, Aeio (0.0285)	Peru, Aeio (0.0062)	G55H, E65K
TLDC1	Lodi, Peru, Aeio (0.0249)	Lodi, Aeio (0.0144)	V188M
F234A	Lodi, Peru (0.0244)	Lodi, Peru (0.0003)	E225G, V311A
HBAD	Lodi, Peru, Aeio (<0.0001)*; Lodi, Aeio (<0.0001)*	Lodi, Aeio (<0.0001)*	P50Q, V55I, G67T, T68N, L73I, L80M
RN115	Lodi, Peru, Aeio (0.0460); Lodi, Peru (0.0460)	Lodi, Peru (0.0131)	V97I
NOL11	Lodi, Peru, Aeio (<0.0001)*; Lodi, Peru (<0.0001)*; Lodi, Aeio (0.0003)*; Peru, Aeio (0.005); Lodi (<0.0001)*; Peru (<0.0001)*; Aeio (0.0443)	Lodi, Peru (0.014)	A53V
CC018	Lodi, Peru, Aeio (<0.0001)*; Lodi, Aeio (<0.0001)*; Peru, Aeio (<0.0001)*; Peru (0.0076); Aeio (<0.0001)*	Peru, Aeio (0.0289)	M57E
MMP28	Lodi, Peru (0.012)	Lodi, Peru (0.0002)	G329S, A334T
HDAC8	Lodi, Peru, Aeio (0.0456); Peru, Aeio (0.0283)	Peru, Aeio (0.026)	P356A
Z3H7A	Lodi, Peru, Aeio (0.0440); Lodi, Aeio (0.0199); Lodi (0.0354)	Lodi, Aeio (0.0104)	I114V
ATAD1	Lodi, Peru (0.0355); Peru (0.0023)	Lodi, Aeio (0.01)	H325Y
COQ9	Lodi, Peru, Aeio (0.0331)	Lodi, Aeio (0.0226)	I142V
TLR21	Lodi, Peru, Aeio (0.0021); Peru, Aeio (0.0005)*; Aeio (0.0179)	Peru, Aeio (0.0002)	K248N, R278Q
CLIP4	Lodi, Peru (0.0167)	Lodi, Peru (0.0068)	I87V
PITM2	Lodi, Peru, Aeio (0.0056); Peru, Aeio (0.0013)	Peru, Aeio (0.0016)	A569S
CCDC6	Lodi, Peru, Aeio (<0.0001)*; Lodi, Peru (<0.0001)*; Peru (0.0002)*	Lodi, Peru (0.0043)	R313S
YCP6	Lodi, Peru, Aeio (0.0023); Lodi, Aeio (0.0023)	Lodi, Aeio (0.0188)	A124I, I174L
LAT4	Peru, Aeio (0.0163)	Peru, Aeio (0.0032)	E66D
D2HDH	Lodi, Peru, Aeio (0.0498); Lodi, Aeio (0.0137)	Lodi, Aeio (0.0197)	A249D
TWF1	Lodi, Peru, Aeio (0.0142); Lodi, Aeio (0.0019)	Lodi, Aeio (0.0005)	Q8K, A9T
SFTPA	Lodi, Peru, Aeio (0.0043); Peru, Aeio (0.0043)	Peru, Aeio (<0.0001)*	I81M, S96K, A101T, V103L, N118S, L157P, G158S, S165N, Q170K
CNTRL	Lodi, Peru, Aeio (0.0048); Lodi, Aeio (0.0017)	Lodi, Peru (0.0173)	P1157S

RRFM	Lodi, Peru, Aeio (0.0175); Peru, Aeio (0.0092)	Peru, Aeio (<0.0001)*	H16L, S18P, F20L, M22V, G23S, G25A, L36P, E39Q, Q84E, N86S
MYOZ1	Lodi, Peru, Aeio (0.0035); Peru, Aeio (0.0006)*	Peru, Aeio (0.0034)	G121A
AL3A2	Lodi, Peru, Aeio (0.0247)	Lodi, Peru (<0.0001)*	H250D, G255S, R256Q
RL35	Lodi, Aeio (0.0199)	Lodi, Aeio (0.0143)	D25E
PTCD1	Lodi, Peru (0.0486)	Lodi, Peru (0.0063)	Q193H
OCAD2	Lodi, Peru, Aeio (0.0300); Lodi, Peru (0.0341)	Lodi, Peru (0.0111)	R3W
MYO19	Lodi, Peru, Aeio (0.0012); Lodi, Aeio (0.0047)	Lodi, Peru (0.0223)	P7L
SYK	Peru, Aeio (0.0339)	Peru, Aeio (0.0045)	I224V
		Lodi, Peru (0.0171)	I348V
CYP2R1	Lodi, Peru, Aeio (0.0025)	Lodi, Aeio (0.0148)	I348V
		Peru, Aeio (0.0148)	I348V
OGG1	Lodi, Aeio (0.0326)	Lodi, Aeio (0.0044)	A122T
DPM1	Peru, Aeio (0.0102)	Peru, Aeio (0.0202)	E143Q
EPS15	Lodi, Peru (0.0353)	Lodi, Peru (0.0017)	S588C
RUSD3	Lodi, Peru, Aeio (0.0084); Lodi, Aeio (0.0009)	Lodi, Aeio (0.0001)*	P196L, T197I
MNT	Lodi, Aeio (0.0291)	Lodi, Aeio (0.0033)	V519M
D19L3	Lodi, Peru, Aeio (0.0271); Lodi, Peru (0.0024); Peru (0.0112)	Lodi, Peru (0.0069)	M698T
CEP89	Lodi, Peru (0.0351)	Lodi, Peru (0.0034)	A242T
HRSL1	Lodi, Peru, Aeio (<0.0001)*; Lodi, Peru (<0.0001)*	Lodi, Peru (<0.0001)*	W92L, I93V, D94G, R95K, D100N, L102I, G103T, S104K
BAT1	Lodi, Peru (0.0299)	Lodi, Peru (0.0042)	I278V
ACSM3	Lodi, Peru, Aeio (0.0006)*; Lodi, Peru (0.0001)*	Lodi, Peru (<0.0001)*	V277A, A279S, W281Y, L284V, A286S, K309E
DHPR	Peru, Aeio (0.0135)	Peru, Aeio (0.0105)	A93T
CD151	Lodi, Peru, Aeio (0.0317); Peru, Aeio (0.0128)	Peru, Aeio (0.0171)	T163S
TM182	Lodi, Peru, Aeio (0.0066); Lodi, Aeio (0.0066)	Lodi, Aeio (0.0132)	A195S
Z518B	Lodi, Peru, Aeio (0.0187); Lodi, Peru (0.0061); Peru, Aeio (0.0025); Peru (0.0065)	Lodi, Peru (0.0322)	V792I
TRAK2	Lodi, Peru, Aeio (<0.0001)*; Lodi, Peru (0.0038); Lodi, Aeio (0.0025); Peru, Aeio (0.0071); Peru (0.0137)	Lodi, Aeio (0.0185)	N8S

AINX	Lodi, Peru, Aeio (<0.0001)*; Lodi, Aeio (<0.0001)*	Lodi, Aeio (0.0138)	A13S
LMCD1	Lodi, Peru, Aeio (0.0004)*; Peru, Aeio (0.0004)*	Peru, Aeio (<0.0001)*	Q170H, S178R, C243F
QCR9	Peru, Aeio (0.0156)	Peru, Aeio (<0.0001)*	S12A, T17S, L30V, V34A, G38A, E48Q
CAVN2	Lodi, Aeio (0.0437)	Lodi, Aeio (0.0307)	G348S
TTHY	Lodi, Peru, Aeio (0.0002)*; Lodi, Aeio (0.0002)*	Lodi, Aeio (0.0004)	H30Y, G74R
NTCP2	Lodi, Peru, Aeio (0.0312); Lodi, Peru (0.0071)	Lodi, Peru (0.0001)*	I115V, F243L
SFXN4	Lodi, Peru (0.0399)	Lodi, Peru (0.0092)	I157V
SMC4	Lodi, Aeio (0.0383)	Lodi, Aeio (0.0015)	S512A
NT5D3	Lodi, Peru, Aeio (0.0336); Lodi, Peru (0.0257)	Lodi, Peru (0.0058)	E262D
RSRC1	Lodi, Peru, Aeio (0.0471); Lodi, Peru (0.0438)	Lodi, Peru (0.0027)	G136A
T4S18	Peru, Aeio (0.0350)	Peru, Aeio (0.0037)	A35T
Y956_13794	Lodi, Peru, Aeio (<0.0001)*; Lodi, Peru (0.0012); Peru, Aeio (0.0078)	Peru, Aeio (0.0374)	V38L
PHAG1	Lodi, Peru (0.0321)	Lodi, Peru (0.0005)	S119N
RN146	Lodi, Peru, Aeio (0.0447); Lodi, Aeio (0.0099)	Lodi, Aeio (<0.0001)*	R307H, A320V, G324E
PR40A	Lodi, Peru, Aeio (0.0023); Peru, Aeio (0.0004)*	Peru, Aeio (0.0066)	V725L
MGST1	Lodi, Aeio (0.0256)	Lodi, Aeio (0.0043)	F41Y, Y66F
CX7A2	Lodi, Peru, Aeio (0.0004)*; Lodi, Aeio (0.0004)*	Lodi, Aeio (0.0003)	R9H, I11V, T15A, A24F
CCD91	Lodi, Aeio (0.0133)	Lodi, Aeio (0.0216)	P129S
RT35	Lodi, Peru, Aeio (0.0020); Lodi, Peru (0.0010)	Lodi, Peru (0.0007)	Q149R, G171S
TSK	Lodi, Peru, Aeio (0.0499); Lodi, Peru (0.0208)	Lodi, Peru (0.0006)	V202I
		Lodi, Peru (0.01)	A413S
L2HGDH	Lodi, Peru, Aeio (<0.0001)*; Lodi, Peru (0.0033)	Lodi, Aeio (0.0067)	A413S
		Peru, Aeio (0.0035)	A413S
LFA3	Lodi, Peru, Aeio (<0.0001)*; Lodi, Peru (0.0186); Lodi, Aeio (<0.0001)*; Lodi (0.0017)	Lodi, Aeio (0.003)	N119S, E126R
ADPRH	Lodi, Peru, Aeio (<0.0001)*; Lodi, Peru (<0.0001)*	Lodi, Peru (0.0353)	Y36N

MFSD5	Lodi, Peru, Aeio (0.0178); Lodi, Peru (0.0075)	Lodi, Peru (0.0012)	G198S
AAAD	Lodi, Peru, Aeio (<0.0001)*; Lodi, Peru (0.0001)*; Lodi, Aeio (<0.0001)*; Lodi (0.0001)*	Lodi, Aeio (0.0267)	P287A
CCS	Lodi, Aeio (0.0087)	Lodi, Aeio (0.0073)	A15T
VCO3	Lodi, Aeio (0.0003)*	Lodi, Aeio (0.006)	P24A, F37L
C1QA	Lodi, Peru, Aeio (<0.0001)*; Lodi, Peru (<0.0001)*; Lodi (0.0107)	Lodi, Peru (0.0006)	M55T, S168I
TOIP1	Lodi, Peru, Aeio (0.0313); Peru, Aeio (0.0025)	Peru, Aeio (0.0158)	R117K
TMOD4	Peru, Aeio (0.0059)	Peru, Aeio (<0.0001)*	I80L, N103D, Q137R, D141E, T145E, Q147L, Q167G
KAD6	Lodi, Peru, Aeio (0.0009)*; Lodi, Peru (0.0003)*; Lodi, Aeio (<0.0001)*; Lodi (<0.0001)*	Lodi, Peru (0.0146)	D42E
ZPI	Lodi, Peru, Aeio (0.0096); Lodi, Aeio (0.0020)	Lodi, Aeio (<0.0001)*	F97L, L104I

"*" indicates genes having conservative statistical significance (FDR < 0.1). The position of convergent amino acid substitution was determined based on the coding sequence of *Taeniopygia guttata*. Lodi, *L. dichrous*; Peru, *Pe. rubidiventris*; Aeio, *A. iouschistos*.

Table S8. Adaptively convergent genes under positive selection with the same amino acid substitutions across all 3 high-altitude tit species.

Gene	Full gene name	Convergent amino acid substitution	Gene function
CYP2R1	Cytochrome P450 family 2 subfamily R member 1	I315V	Synthesis of cholesterol, steroids and other lipids
L2HGDH	L-2-hydroxyglutarate dehydrogenase	A402S	A FAD-dependent enzyme
HN1L	Hematological and neurological expressed 1 like	Q183R	Apoptosis modulation and signaling
IFNAR2	Interferon alpha and beta receptor subunit 2	R114Q	Phosphorylation of several proteins

The position of convergent amino acid substitution was determined based on the coding sequence of *T. guttata*. Gene function was identified through GeneCards database (www.genecards.org).

Table S9. Comparisons of coefficient of variance based on gene expression levels among all samples before and after normalization, for all genes, conserved genes, and nonconserved gene.

Gene set	Mann–Whitney *U* test (W)	*P* value
All genes	25,817,000	2.5e-5
Conserved genes	688,610	< 2.2e-16
Nonconserved genes	18,971,000	1.9 e-4

Table S10. One-way ANOVAs for the PCA axes for all samples across the 5 tissues across the 6 tit species, and showing the first 2 axes.

	Tissue			Species		
	$F_{4,128}$	*P* value	FDR	$F_{5,128}$	*P* value	FDR
PC1	3,558.318	< 2e-16 ***	< 2e-16 ***	0.023	1	1
PC2	1,934.679	< 2e-16 ***	< 2e-16 ***	0.098	0.992	1

Significance levels, ***P value (FDR) < 0.001, **P value (FDR) < 0.01, and *P value (FDR) < 0.05.

Table S11. Pearson's correlation coefficients between module expression and phenotypic traits.

Tissue	Module	Body length	Body weight	Culmen length	Tail length	Tarsus length	Wing length
Lung	2	−0.44 (4.19e-2)	0.22 (3.16e-1)	0.16 (4.76e-1)	−0.46 (3.30e-2)	−0.58 (4.31e-3)	−0.19 (3.85e-1)
	5	0.76 (4.85e-5)	0.31 (1.63e-1)	0.38 (8.10e-2)	0.37 (8.70e-2)	0.51 (1.49e-2)	0.56 (7.27e-3)
	6	0.79 (1.02e-5)	0.13 (5.73e-1)	0.20 (3.65e-1)	0.47 (2.55e-2)	0.83 (1.44e-6)	0.62 (2.25e-3)
	9	0.30 (1.70e-1)	0.46 (3.30e-2)	0.56 (6.57e-3)	−0.23 (3.07e-1)	0.54 (9.17e-3)	0.70 (2.99e-4)
	25	−0.68 (4.93e-4)	0.07 (7.58e-1)	−0.11 (6.17e-1)	−0.59 (3.87e-3)	−0.44 (3.92e-2)	−0.22 (3.31e-1)
Cardiac muscle	3	0.83 (6.32e-8)	0.27 (1.72e-1)	0.32 (1.02e-1)	0.57 (1.69e-3)	0.55 (2.25e-3)	0.54 (2.78e-3)
	20	−0.43 (2.10e-2)	0.10 (6.12e-1)	0.13 (5.07e-1)	−0.45 (1.53e-2)	−0.49 (7.68e-3)	−0.22 (2.51e-1)
	21	−0.77 (1.61e-6)	−0.09 (6.64e-1)	−0.07 (7.36e-1)	−0.60 (6.97e-4)	−0.84 (2.63e-8)	−0.54 (2.79e-3)
Kidney	2	−0.62 (2.30e-3)	0.15 (5.06e-1)	−0.02 (9.26e-1)	−0.57 (5.54e-3)	−0.49 (1.99e-2)	−0.19 (3.99e-1)
	3	−0.83 (2.09e-6)	−0.13 (5.70e-1)	−0.19 (4.06e-1)	−0.49 (1.99e-2)	−0.87 (1.37e-7)	−0.63 (1.53e-3)
	9	0.38 (7.87e-2)	0.44 (3.92e-2)	0.53 (1.10e-2)	−0.17 (4.42e-1)	0.62 (2.23e-3)	0.72 (1.37e-4)
	12	0.82 (2.51e-6)	0.31 (1.60e-1)	0.40 (6.69e-2)	0.47 (2.55e-2)	0.50 (1.69e-2)	0.55 (7.55e-3)
	17	0.46 (3.15e-2)	−0.60 (3.18e-3)	−0.59 (3.83e-3)	0.78 (1.70e-5)	0.55 (8.02e-3)	−0.14 (5.42e-1)
Liver	6	0.25 (2.05e-1)	0.32 (9.74e-2)	0.43 (2.29e-2)	−0.17 (3.98e-1)	0.50 (7.13e-3)	0.55 (2.32e-3)
	8	−0.77 (1.64e-6)	−0.32 (1.00e-1)	−0.39 (4.24e-2)	−0.47 (1.16e-2)	−0.55 (2.28e-3)	−0.59 (9.54e-4)
	10	−0.51 (5.50e-3)	0.15 (4.33e-1)	0.18 (3.60e-1)	−0.54 (2.85e-3)	−0.57 (1.43e-3)	−0.24 (2.09e-1)
	17	−0.66 (1.47e-4)	−0.50 (6.22e-3)	−0.45 (1.74e-2)	−0.18 (3.66e-1)	−0.80 (3.77e-7)	−0.83 (6.58e-8)
	21	−0.53 (4.00e-3)	0.24 (2.09e-1)	0.06 (7.43e-1)	−0.58 (1.15e-3)	−0.43 (2.15e-2)	−0.12 (5.29e-1)
	22	−0.53 (3.52e-3)	0.47 (1.12e-2)	0.51 (5.95e-3)	−0.82 (9.90e-8)	−0.58 (1.28e-3)	0.01 (9.71e-1)
Flight muscle	2	0.36 (6.08e-2)	0.37 (5.31e-2)	0.47 (1.15e-2)	−0.13 (4.96e-1)	0.61 (6.37e-4)	0.67 (8.94e-5)
	14	0.49 (8.49e-3)	−0.52 (4.30e-3)	−0.57 (1.49e-3)	0.80 (3.79e-7)	0.59 (8.84e-4)	−0.04 (8.31e-1)
	15	−0.80 (4.21e-7)	−0.27 (1.72e-1)	−0.36 (5.85e-2)	−0.53 (3.98e-3)	−0.53 (3.94e-3)	−0.54 (3.29e-3)
	16	−0.50	0.18	−0.02	−0.49	−0.41	−0.17

		(6.29e-3)	(3.71e-1)	(9.17e-1)	(7.82e-3)	(2.99e-2)	(3.86e-1)
	17	−0.80	0.04	−0.01	−0.65	−0.84	−0.47
		(3.97e-7)	(8.20e-1)	(9.43e-1)	(2.07e-4)	(2.92e-8)	(1.07e-2)

Note that the corresponding *P* value of Pearson's correlation coefficient is shown in the bottom parenthesis.

Table S12. Effects of altitude, ortholog expression, and connectivity on the dN/dS ratio using linear models.

Formula	Explanatory variables	Coefficients	*P* value
log(dNdS) ~ Altitude	Altitude	0.0396	2.11e-1
log(dNdS) ~ log(Expression)	log(Expression)	−0.1069	<2e-16 ***
log(dNdS) ~ log(Connectivity)	log(Connectivity)	−0.0538	7.75e-6 ***
log(dNdS) ~ log(Expression)*Altitude + log(Connectivity)*Altitude	Altitude	−0.0614	5.49e-1
	log(Expression)	−0.1422	1.45e-8 ***
	log(Connectivity)	0.0481	1.10e-1
	log(Expression) + Altitude	0.0578	4.74e-2 *
	log(Connectivity) + Altitude	−0.0865	9.31e-3 **

Significance levels, ****P* value < 0.001, ***P* value < 0.01, and **P* value < 0.05.

Additional data table S1 (separate file)

List of differentially expressed genes shared among the 3 high- and low-altitude species pairs in lung, cardiac muscle, kidney, liver, and flight muscle. Genes with significantly higher or lower expression values in the high-altitude species compared to their respective low-altitude species were up-regulated or down-regulated. Gene function was identified through GeneCards database (www.genecards.org).

References

1. del Hoyo J, Elliott A, Sargatal J, Christie D, de Juana E (2018) *Handbook of the birds of the world alive* (Lynx Edicions, Barcelona).
2. Li G, Zheng B, Liu G (1982) *Fauna Sinica*: *Aves* (Science Press, Beijing).
3. Zhu X, et al. (2018) Divergent and parallel routes of biochemical adaptation in high-altitude passerine birds from the Qinghai-Tibet plateau. *Proc Natl Acad Sci USA* 115:1865–1870.
4. Hochachka PW, Rupert JL, Monge C (1999) Adaptation and conservation of physiological systems in the evolution of human hypoxia tolerance. *Comp Biochem Physiol A Mol Integr Physiol* 124:1–17.
5. Hochachka PW (1998) Mechanism and evolution of hypoxia-tolerance in humans. *J Exp Biol* 201:1243–1254.
6. Chen Y, et al. (2018) SOAPnuke: A MapReduce acceleration-supported software for integrated quality control and preprocessing of high-throughput sequencing data. *GigaScience* 7:gix120–gix120.
7. Haas BJ, et al. (2013) *De novo* transcript sequence reconstruction from RNA-seq using the Trinity platform for reference generation and analysis. *Nat Protoc* 8:1494–1512.
8. Fu L, Niu B, Zhu Z, Wu S, Li W (2012) CD-HIT: Accelerated for clustering the next-generation sequencing data. *Bioinformatics* 28:3150–3152.
9. Langmead B, Salzberg SL (2012) Fast gapped-read alignment with Bowtie 2. *Nat Methods* 9:357–359.
10. Simão FA, Waterhouse RM, Ioannidis P, Kriventseva EV, Zdobnov EM (2015) BUSCO: Assessing genome assembly and annotation completeness with single-copy orthologs. *Bioinformatics* 31:3210–3212.
11. Li B, Dewey CN (2011) RSEM: Accurate transcript quantification from RNA-Seq data with or without a reference genome. *BMC Bioinformatics* 12:323.
12. Warren WC, et al. (2010) The genome of a songbird. *Nature* 464:757–762.
13. Selvatti AP, Gonzaga LP, Russo CA (2015) A Paleogene origin for crown passerines and the diversification of the Oscines in the New World. *Mol Phylogenet Evol* 88:1–15.
14. Zerbino DR, et al. (2018) Ensembl 2018. *Nucleic Acids Res* 46:D754–D761.
15. Gotz S, et al. (2008) High-throughput functional annotation and data mining with the Blast2GO suite. *Nucleic Acids Res* 36:3420–3435.
16. Moriya Y, Itoh M, Okuda S, Yoshizawa AC, Kanehisa M (2007) KAAS: An automatic genome annotation and pathway reconstruction server. *Nucleic Acids Res* 35:W182–W185.
17. Slater GS, Birney E (2005) Automated generation of heuristics for biological sequence comparison. *BMC Bioinformatics* 6:31.
18. Löytynoja A, Goldman N (2008) Phylogeny-aware gap placement prevents errors in sequence alignment and evolutionary analysis. *Science* 320:1632–1635.
19. Fletcher W, Yang Z (2010) The effect of insertions, deletions, and alignment errors on the branch-site test of positive selection. *Mol Biol Evol* 27:2257–2267.
20. Castresana J (2000) Selection of conserved blocks from multiple alignments for their use in phylogenetic analysis. *Mol Biol Evol* 17:540–552.
21. Eyre-Walker A, Keightley PD (1999) High genomic deleterious mutation rates in hominids. *Nature* 397:344.
22. Nachman MW, Crowell SL (2000) Estimate of the mutation rate per nucleotide in humans. *Genetics* 156:297–304.
23. Darriba D, Taboada GL, Doallo R, Posada D (2012) jModelTest 2: More models, new heuristics and parallel computing. *Nat Methods* 9:772–772.
24. Stamatakis A (2014) RAxML version 8: A tool for phylogenetic analysis and post-analysis of large phylogenies. *Bioinformatics* 30:1312–1313.
25. Yang Z (2007) PAML 4: Phylogenetic analysis by maximum likelihood. *Mol Biol Evol*

24:1586–1591.
26. Axelsson E, et al. (2008) Natural selection in avian protein-coding genes expressed in brain. *Mol Ecol* 17:3008–3017.
27. Zhang J, Kumar S (1997) Detection of convergent and parallel evolution at the amino acid sequence level. *Mol Biol Evol* 14:527–536.
28. Zou Z, Zhang J (2015) Are convergent and parallel amino acid substitutions in protein evolution more prevalent than neutral expectations? *Mol Biol Evol* 32:2085–2096.
29. Robinson MD, McCarthy DJ, Smyth GK (2009) edgeR: A Bioconductor package for differential expression analysis of digital gene expression data. *Bioinformatics* 26:139–140.
30. Brawand D, et al. (2011) The evolution of gene expression levels in mammalian organs. *Nature* 478:343–348.
31. Harrison PW, et al. (2015) Sexual selection drives evolution and rapid turnover of male gene expression. *Proc Natl Acad Sci USA* 112:4393–4398.
32. Benjamini Y, Hochberg Y (1995) Controlling the false discovery rate: A practical and powerful approach to multiple testing. *J R Stat Soc B* 57:289–300.
33. Storey JD, Tibshirani R (2003) Statistical significance for genomewide studies. *Proc Natl Acad Sci USA* 100:9440–9445.
34. Paradis E, Claude J, Strimmer K (2004) APE: Analyses of phylogenetics and evolution in R language. *Bioinformatics* 20:289–290.
35. Love MI, Huber W, Anders S (2014) Moderated estimation of fold change and dispersion for RNA-seq data with DESeq2. *Genome Biol* 15:550.
36. Poisot T, et al. (2017) ROTS: An R package for reproducibility-optimized statistical testing. *PLoS Comput Biol* 13:e1005562.
37. Ritchie ME, et al. (2015) Limma powers differential expression analyses for RNA-sequencing and microarray studies. *Nucleic Acids Res* 43:e47.
38. Langfelder P, Horvath S (2008) WGCNA: An R package for weighted correlation network analysis. *BMC Bioinformatics* 9:559.